EUROPEAN RESPIRATORY journal

FLAGSHIP SCIENTIFIC JOURNAL OF ERS

Early View

Original article

Phospholipase A2-Receptor 1 Promotes Lung-Cell Senescence and Emphysema in Obstructive Lung Disease

Delphine Beaulieu, Aya Attwe, Marielle Breau, Larissa Lipskaia, Elisabeth Marcos, Emmanuelle Born, Jin Huang, Shariq Abid, Geneviève Derumeaux, Amal Houssaini, Bernard Maitre, Marine Lefevre, Nora Vienney, Philippe Bertolino, Sara Jaber, Hiba Noureddine, Delphine Goehrig, David Vindrieux, David Bernard, Serge Adnot

Please cite this article as: Beaulieu D, Attwe A, Breau M, *et al*. Phospholipase A2-Receptor 1 Promotes Lung-Cell Senescence and Emphysema in Obstructive Lung Disease. *Eur Respir J* 2021; in press (https://doi.org/10.1183/13993003.00752-2020).

Phospholipase A2-Receptor 1 Promotes Lung-Cell Senescence and Emphysema in Obstructive Lung Disease

Delphine Beaulieu[1], Aya Attwe[1, 4], Marielle Breau[1], Larissa Lipskaia[1], Elisabeth Marcos[1], Emmanuelle Born[1], Jin Huang[1], Shariq Abid[1], Geneviève Derumeaux[1], Amal Houssaini[1], Bernard Maitre[1], Marine Lefevre[2], Nora Vienney[1], Philippe Bertolino[3], Sara Jaber[3], Hiba Noureddine[4], Delphine Goehrig[3], David Vindrieux[3], David Bernard[3], Serge Adnot[1*]

David Bernard and Serge Adnot are co-senior authors of this study.
Delphine Beaulieu and Aya Attwe contributed equally to this study.

[1]INSERM U955, Département de Physiologie-Explorations Fonctionnelles, and DHU A-TVB Hôpital Henri Mondor, AP-HP, 94010, Créteil, France
[2] Institut Mutualiste Montsouris, Département anatomopathologie, Paris, France
[3]Centre de Recherche en Cancérologie de Lyon, UMR INSERM U1052/CNRS 5286, Université de Lyon, Centre Léon Bérard, Lyon, France
[4]Environmental Health Research Lab (EHRL), Faculty of Sciences V, Lebanese University, Nabatieh, Lebanon.

Correspondence should be addressed to Serge Adnot, Hôpital Henri Mondor, Service de Physiologie-Explorations Fonctionnelles, 94010, Créteil, France.
Tel: +33 149 812 677; Fax: +33 149 812 667; E-mail: serge.adnot@inserm.fr

Running head: PLA2R1 and Cell Senescence in COPD

Word count: 3 328
This article has an online data supplement

PLA2R1 is a potent regulator of lung-cell senescence in COPD, with JAK/STAT signaling as a major effector. Pharmacological inhibition of JAK1/2 attenuates PLA2R1-induced lung alterations in murine models. Targeting JAK1/2 may represent a promising therapeutic approach for COPD.

Abstract

Rationale. Cell senescence is a key process in age-associated dysfunction and diseases, notably chronic obstructive pulmonary disease (COPD). We previously identified phospholipase A2-receptor 1 (PLA2R1) as a positive regulator of cell senescence acting via JAK/STAT signaling. Its role in pathology, however, remains unknown. Here, we assessed PLA2R1-induced senescence in COPD and lung emphysema pathogenesis.

Methods. Assessment of cell senescence in lungs and cultured lung cells from patients with COPD and controls subjected to PLA2R1 knock-down, *PLA2R1* gene transduction and treatment with the JAK1/2 inhibitor ruxolitinib. To assess whether *PLA2R1* upregulation caused lung lesions, we developed transgenic mice overexpressing *PLA2R1* (*PLA2R1*-TG) and intratracheally injected wild-type mice with a lentiviral vector carrying the *PLA2R1* gene (LV-*PLA2R1* mice).

Measurements and Results. We found that *PLA2R1* was overexpressed in various cell types exhibiting senescence characteristics in COPD lungs. *PLA2R1* knockdown extended the population doubling capacity of these cells and inhibited their proinflammatory senescence-associated secretory phenotype (SASP). PLA2R1-mediated cell senescence in COPD was largely reversed by treatment with the potent JAK1/2 inhibitor ruxolitinib. Five month-old *PLA2R1*-TG mice exhibited lung-cell senescence and developed lung emphysema and lung fibrosis together with pulmonary hypertension. Treatment with ruxolitinib induced reversal of lung emphysema and fibrosis. LV-*PLA2R1*-treated mice developed lung emphysema within four weeks, and this was markedly attenuated by concomitant ruxolitinib treatment.

Conclusion. Our data support a major role for PLA2R1 activation in driving lung-cell senescence and lung alterations in COPD. Targeting JAK1/2 may represent a promising therapeutic approach for COPD.

Keywords: PLA2R1, cell senescence, lung disease, emphysema, COPD

Introduction

Exaggerated lung-cell senescence is now emerging as a key pathogenic factor in several chronic respiratory diseases [1], notably chronic obstructive pulmonary disease (COPD), a major cause of morbidity and mortality in most countries for which no curative treatment is available [2-4]. COPD is characterized by slowly progressive airflow obstruction and emphysema due to lung parenchyma destruction developing in association with chronic lung inflammation [5]. We previously reported that a characteristic feature of COPD is the accumulation of senescent cells in the lung, which limits the potential for tissue renewal and contributes to chronic inflammation through the senescence-associated secretory phenotype (SASP) [4, 6, 7]. In COPD, exaggerated lung-cell senescence may result from a combination of replicative cell senescence due to telomere shortening and of premature cell senescence caused by various stress stimuli such as oxidative stress and inflammatory mediators [8-10]. These processes engage a DNA damage response with p53-dependent upregulation of the cyclin-dependent-kinase inhibitor p21 and expression of p16INK4A [10, 11].

A causal relationship between cell senescence and the lung manifestations of COPD is now supported by several studies. Some cases of familial lung emphysema are related to a loss-of-function mutation in the telomerase *TERT* gene and are therefore classified as telomere disorders [12]. Moreover, individuals with short telomeres experience an accelerated decline in lung function [13]. In mouse models, interventions that delay or inhibit cell senescence protect against cigarette smoke-induced lung emphysema, bronchial remodeling, and inflammation [14, 15]; whereas accelerated lung-cell senescence promotes some of the lung alterations seen in COPD [7]. Consequently, there is an urgent need for identifying molecular pathways that are relevant to the lung-cell senescence program in COPD and that could be targeted pharmacologically.

In previous studies, we identified phospholipase-A2-receptor-1 (PLA2R) as a crucial regulator of both replicative- and stress-induced cell senescence [16]. PLA2R1, a transmembrane protein belonging to the C-type lectin receptor superfamily and the mannose receptor family, binds a few secreted phospholipase-A2s (sPLA2s), various collagen types, and carbohydrate [17]. Recent studies by our groups indicate that an important function of PLA2R1 is related to its prosenescent effect, which seems to be sPLA2-independent [18] and involves the JAK/STAT signaling pathway [19-23].

Here, we explored the potential importance of PLA2R1 and JAK/STAT signaling in lung-cell senescence and COPD. We observed that PLA2R1 overexpression was a major mechanism leading to lung-cell senescence in COPD and that lung PLA2R1 overexpression in mice induced lung-cell senescence and lung alterations, including lung emphysema, lung fibrosis, and pulmonary hypertension. Treatment with the JAK1/2 inhibitor ruxolitinib delayed the senescence process in cells from patients with COPD, inhibited the SASP, and attenuated the pathological lung alterations resulting from PLA2R1 overexpression in mice. Targeting PLA2R1 and/or the JAK/STAT pathway may represent a new therapeutic strategy for inhibiting lung-cell senescence in COPD.

METHODS

Patients and controls

The study was approved by the institutional review board of the Henri Mondor Teaching Hospital, Créteil, France. All patients and controls signed an informed consent document before study inclusion.

Lung tissue samples were obtained from 46 patients who underwent lung resection surgery at the *Institut Mutualiste Montsouris*, Paris, France. Among them, 23 had COPD and 23 were control smokers matched to the COPD patients on age and sex (Table 1). Inclusion criteria for the patients with COPD were an at least 10 pack-year smoking history and a ratio of forced expiratory volume in 1 second (FEV_1) over forced vital capacity (FVC) <70%. The controls had to have a smoking history greater than 5 pack-years; an FEV_1/FVC ratio greater than 70%; and no evidence of chronic cardiovascular, hepatic, or renal disease.

Animal studies

Adult male mice (C57Bl/6j) were used according to institutional guidelines, which complied with national and international regulations (agreement #94-28245). Pulmonary arterial hypertension, lung emphysema, and lung tissue analysis were performed according to the standard techniques detailed in the online supplement.

The online supplement provides details of the studies performed on lung samples and cultured cells from patients and controls, on animal studies, and on the statistical analysis.

RESULTS

PLA2R1 is overexpressed in lungs and derived cultured cells from patients with COPD

To investigate *PLA2R1* expression and lung-cell senescence in COPD, we studied lung tissues from 23 patients with COPD and 23 controls, as well as derived lung cells from a subset of 8 patients and 10 controls (Supplementary Tables S1 and S2). Compared to control lungs, lungs from patients with COPD had higher protein levels of PLA2R1, p21, and p16 (Fig. 1a). Immunofluorescence studies of lungs from patients with COPD revealed prominent PLA2R1 staining in pulmonary vascular endothelial cells (P-ECs), pulmonary-artery smooth muscle cells (PA-SMCs), and alveolar epithelial type II cells (AECs), all of which also stained for p16 (Fig. 1b,c and supplemental Fig.1) and for the DNA damage markers p-γH2AX and 53BP1 (Fig. 2a,b). In contrast, PLA2R1 immunofluorescence was weak in lungs from controls. PLA2R1 mRNA levels were also higher in cultured PA-SMCs and P-ECs from patients with COPD, which exhibited early-onset cell senescence manifesting as fewer population doublings (PDLs) and higher β-galactosidase-positive cell counts compared to those from controls (Fig. 3a, b). PLA2R1 mRNA levels increased in both PA-SMCs and P-ECs from patients and controls during repeated passages (Fig. 3a, b).

Downregulation of *PLA2R1* inhibits cell senescence in COPD

To investigate the effect of *PLA2R1* knockdown on cellular senescence in COPD, we infected cultured PA-SMCs with a retroviral vector encoding an shRNA that targeted PLA2R1 (shPLA2R1) [16]. PLA2R1 mRNA levels were decreased by about 80% in cells stably infected with the shPLA2R1-encoding vector, compared to cells infected with the control vector (Supplementary Fig. 2). *PLA2R1* knockdown consistently decreased the number of β-galactosidase-positive cells and increased the PDL to a greater extent in cells from patients with COPD (9-fold increase) than in those from controls (2-fold increase) (Fig.

4a, b). In addition, p16 and p21 protein levels were decreased in cells from both patients with COPD and controls (Fig. 4c). *PLA2R1* knockdown reduced the levels of the SASP components tested, notably in cells from patients with COPD, which released large amounts of IL-8, IL-6, and PAI-1 (Fig. 4d).

To better assess the effect of *PLA2R1* knockdown on cell senescence in COPD, we then compared the effects of *PLA2R1* versus *p53* knockdown in PA-SMCs from a subset of 5 patients and 5 controls. Compared to cells infected with the vector encoding shPLA2R1, cells infected with the shp53 vector exhibited a similar PDL increase and a similar decrease in the percentage of β-galactosidase-positive cells (Supplementary Fig. 3a). The levels of p16 and p21 proteins and of SASP components were reduced to a similar extent by both vectors (Supplementary Figs. 3b, c).

JAK inhibition by ruxolitinib reverts *PLA2R1*-induced cell senescence

To explore the potential role for JAK1/2 on *PLA2R1*-induced cell senescence in primary lung-cell cultures, we examined the effect of ectopic *PLA2R1* expression on cell senescence by using a retroviral vector encoding the *PLA2R1* gene [19]. PA-SMCs from controls with less than 55% of β-galactosidase-positive cells were used. Immunofluorescence studies revealed that cells transduced with the retroviral vector and positive for PLA2R1 stained also for phosphorylated JAK2 and STAT3 (Fig. 5a). These cells became rapidly senescent, as shown by strong p16 immunofluorescence and β-galactosidase staining activity–and an inability to divide, with a low PDL and weak proliferating cell nuclear antigen staining (Fig. 5b, c). Cells infected with the control vector were not stained for p-JAK2 and p-STAT3 (Fig. 5a). We then investigated whether inhibition of JAK2 by the potent JAK1/2 inhibitor ruxolitinib altered *PLA2R1*-induced cell senescence. In cells undergoing cell senescence induced by *PLA2R1* gene transduction,

ruxolitinib treatment almost fully inhibited the response, increasing the PDL, decreasing the percentage of β-galactosidase-positive cells, and returning the levels of the p16 and PCNA staining and of the SASP components IL-8, IL-6, and PAI-1 to basal values (Fig. 5 b, c, d).

Treatment with ruxolitinib attenuates cell senescence and suppresses the SASP in cells from patients with COPD

We then investigated the link between *PLA2R1* expression, cell senescence, and JAK/STAT in lungs and cells from patients with COPD. Immunofluorescence studies revealed strong PLA2R1 and JAK2 staining that co-localized in various cell types from COPD lungs, contrasting with weak JAK2 staining in control lungs (Fig. 6a). Strong immunostaining for p-STAT3 was also found in lungs from patients with COPD (Fig. 6b). JAK1 staining was undetectable. Ruxolitinib treatment of PA-SMCs from patients with COPD and controls increased the PDL and decreased the percentage of β-galactosidase-positive cells, although these effects were weaker than those produced by *PLA2R1* knockdown (Fig. 6c). Strikingly, ruxolitinib potently suppressed the SASP of senescent cells from patients with COPD, as shown by decreases in the release of IL-8, IL-6, and PAI-1, which returned to the basal levels measured in cells from controls (Fig. 6d).

***PLA2R1* overexpression in transgenic mice induces lung-cell senescence and structural lung alterations, which can be reversed by ruxolitinib**

To assess whether lung overexpression of *PLA2R1* replicated some of the lung alterations seen in COPD, we generated transgenic mice that constitutively expressed the human *PLA2R1* gene (*PLA2R1*-TG mice). Five-month-old *PLA2R1*-TG mice displayed an apparently normal phenotype but overexpressed lung hPLA2R1 and p16 protein compared to control mice (Fig. 7a). Lungs from *PLA2R1*-TG mice exhibited strong PLA2R1 and p16

immunofluorescence (Fig. 7a) with increased lung mRNA levels of the JAK/STAT target genes Tap1, Socs1, and Irf7 (Fig. 7b). These changes were associated with diffuse lung emphysema, as quantified by the mean distance separating alveolar septa (mean linear intercept) (Fig. 7c); and with fibrotic lung lesions, as quantified by the Ashcroft score of red Sirius-stained lung sections (Fig. 7d) and by lung mRNA levels of collagens-1 A1, A2, collagen-3 A1, actin alpha 2 (ACTA2), and fibronectin (Fig. 7e). Lung fibrosis in *PLA2R1*-TG mice was also illustrated by increases in Masson trichrome staining (Fig. 7d) and in vimentin and fibroblast-specific protein (FSP) immunostaining (Supplemental Fig. 4. a,b). *PLA2R1*-TG mice also developed pulmonary hypertension, with increases in right ventricular systolic pressure, right heart hypertrophy, and pulmonary vessel muscularization (Supplemental Fig. 5). Other abnormalities consisted of increased lung levels of IL-6, MCP-1, IL-1β, and PAI-1 in lungs from *PLA2R1*-TG mice but not in control mice (Fig. 7f). We then investigated the effect of ruxolitinib treatment in a dose of 75 mg/kg/day for 15 consecutive days. This short-term ruxolitinib treatment reduced lung emphysema and fibrosis parameters, inducing marked reductions in lung p16 protein, JAK/STAT target genes, and SASP members (Fig. 7a, b, c, d, e, f).

Ruxolitinib treatment prevents lung-cell senescence and lung alterations induced by intratracheal delivery of the *PLA2R1* gene

To further investigate the effect of ruxolitinib on lung alterations induced by *PLA2R1* overexpression, we studied mice injected intratracheally with a lentiviral vector encoding the murine *PLA2R1* gene (LV-*PLA2R1*) and given concomitant continuous ruxolitinib treatment (75 mg/kg/day). Preparatory experiments performed with a lentiviral vector encoding the reporter mCherry gene under the control of the CMV promoter (LV-mCherry) revealed that approximately 15% of lung cells were transduced by this procedure including alveolar

epithelial cells (supplemental Fig 6). Gene transfer was efficient, as shown by diffuse PLA2R1 staining activity throughout the lung structures four weeks after LV-*PLA2R1* injection (Fig. 8a). At this time, the mice exhibited marked increases in lung mRNA levels of PLA2R1, p21, and of the JAK/STAT target genes Tap1, Socs1, and Irf7 (Fig. 8b and supplemental Fig. 7a), as well as in lung p21 and p16 protein levels compared to mice injected with the control vector (LV-ncRNA) (Fig. 8c). Most importantly, LV-*PLA2R1* mice developed lung emphysema (Fig. 8d), increases in the right ventricular systolic pressure and hypertrophy index, and pulmonary vessel remodeling (supplemental Fig. 7b, c, d). Ruxolitinib treatment started at the time of LV-*PLA2R1* administration markedly reduced the development of lung emphysema and pulmonary vascular remodeling (Fig. 8d and supplemental Fig. 7b, c, d), while also decreasing JAK/STAT downstream genes and p21 mRNA levels (Fig. 8b and supplemental Fig. 7a) and p21 and p16 protein levels (Fig 8c). No consistent changes were seen in lung cytokine levels four weeks after LV-*PLA2R1* injection.

DISCUSSION

Our data support a major role for *PLA2R1* activation in driving lung-cell senescence and lung alterations in COPD. Here, we showed that *PLA2R1* overexpression was strongly involved in the exaggerated lung-cell senescence seen in COPD and that PLA2R1 overexpression in mice induced lung-cell senescence and pathology. JAK2 activation emerged as an important downstream event to PLA2R1 signaling, notably as a SASP activator. The JAK1/2 inhibitor ruxolitinib delayed the senescence process, inhibiting the SASP in cells from patients with COPD, and also attenuated the pathological lung alterations resulting from *PLA2R1* overexpression in mice. Thus, targeting PLA2R1 and/or the JAK2 pathway may represent a new therapeutic strategy for counteracting lung-cell senescence in COPD.

The potential role for PLA2R1 in pathology remains poorly understood. Until recently, efforts focused on the ability of PLA2R1 to bind soluble PLA2s, which catalyze phospholipid hydrolysis and generate inflammatory lipid mediators [17]. However, the physiological consequences of soluble PLA2s binding to PLA2R1 remain unclear [24], and accumulating evidence now supports an intrinsic role for PLA2R1 in several pathologic conditions [20]. We have reported that *PLA2R1* can act as a tumor suppressor and that its decreased expression in various cancers promotes tumor progression [20, 21], or can promote some progeroid hallmarks [22]. Structure-function studies and chemical inhibition of shPLA2-related signaling pathways revealed that the ability of *PLA2R1* to exert its tumor suppressive effect was independent of sPLA2 [18]. Here, we provide evidence for a new pathogenic role for *PLA2R1* due to *PLA2R1* overexpression in the lung in the context of COPD.

PLA2R1 was overexpressed in several cell types from lungs from COPD patients but was only very weakly expressed in lungs from controls. PLA2R1-stained cells were

senescent, as they also stained for p16, a major onco-suppressor expressed in senescent cells [25], and for 53BP1 and γ-H2AX, two well established DNA damage markers. The prominent and intrinsic role for *PLA2R1* in the senescence process in COPD was further demonstrated by the ability of its knockdown to delay cell senescence in primary cultured cells from patients with COPD, independently of the pathologic environment. We previously showed that cells from patients with COPD, compared to control cells, were characterized by a marked reduction in their PDL and by the release of various inflammatory factors and cytokines as part of the SASP [6, 7]. We show here that *PLA2R1* inactivation not only markedly improved the PDL, but also completely suppressed the SASP.

An interesting point is that *PLA2R1* knockdown was almost as potent as *p53* neutralization in inhibiting cell senescence and suppressing the SASP in cells from patients with COPD. That cell senescence was p53-dependent in COPD was not surprising, given that DNA damage and telomere dysfunction, both of which engage the p53 pathway, are among the main processes responsible for cell senescence in COPD [8, 26, 27]. Moreover, our previous studies suggest that p53 may be downstream of PLA2R1 [16]. Previous studies from our groups also showed that PLA2R1 activated the JAK2 pathway and that this activation mediated at least part of the prosenescent effect of PLA2R1 [19]. Indeed, we showed that inhibition of JAK/STAT signaling by genetic or pharmacological tools reverted PLA2R1 effects [19], whereas inhibition by ruxolitinib phenocopied PLA2R1 loss, delaying senescence and improving premature aging [22, 23]. Our present results are consistent with this finding since lungs from patients with COPD that stained for PLA2R1 also stained strongly for JAK2 and p-STAT3. A JAK-STAT increase was previously reported in lungs from patients with COPD, although its role was not investigated [28]. The JAK2 pathway has been associated with oncogenic effects, but its potential pathogenic role in COPD remained unclear. Here, we found that cells transduced with the *PLA2R1* gene and

undergoing senescence became positive for Phospho-JAK2 and phospho-STAT3. Moreover, pharmacological inhibition of JAK2 with ruxolitinib fully reversed the induction of cell senescence induced by in vitro *PLA2R1* transduction. These results indicate that one major mechanism responsible for JAK/STAT activation in COPD is linked to the senescence process driven by *PLA2R1*.

Previous studies established that JAK activation mediated the SASP in senescent cells from adipose tissue during aging [29]. JAK1/2 inhibitors reduced inflammation and alleviated frailty in aged mice [29]. Similarly, our results support a major effect of the JAK/STAT pathway in promoting the SASP in senescent cells. Moreover, ruxolitinib treatment reversed *PLA2R1*-induced cell senescence and slightly but significantly delayed the onset of cell senescence in cells from patients with COPD. It is unlikely that the ability of ruxolitinib to decrease cell senescence was due to inhibition of the SASP. Indeed, in previous work by our groups, selectively suppressing the inflammatory arm of the SASP, for instance via NF-κB inactivation, did not affect lung-cell senescence in COPD [7]. Our results thus indicate that the JAK2 pathway mediates part of the prosenescent effects of PLA2R1 in COPD, with prominent blunting of the SASP by inhibition of the pathway. However, it is likely that not all the effects of PLA2R1 are mediated via JAK/STAT and also that some of the effects of JAK/STAT inhibition on cell senescence may rely on mechanisms beyond PLA2R1 activation.

To assess whether *PLA2R1*-induced cell senescence played a causal role in COPD, we developed mice overexpressing *PLA2R1*. Although these mice had an apparently normal phenotype, they developed major lung alterations consisting in emphysema and fibrotic lesions at a young age, concomitantly with the accumulation of senescent lung cells stained for both p16 and PLA2R1, increased expression of lung JAK/STAT target genes, and increased expression of SASP members. These mice also developed pulmonary

hypertension, a finding consistent with the reported association between pulmonary hypertension and the development of lung emphysema in mouse models [30]. Taken together, these results in mice show that, even in young mice, PLA2R1 pathway activation is sufficient to drive cell senescence with the concomitant development of lung emphysema and fibrosis. These findings are consistent with recent evidence of a pathogenic role for senescent cells in a murine lung-fibrosis model [31] and with the accumulation of senescent cells in lungs from patients with idiopathic lung fibrosis [32, 33]. The pathogenic role for lung-cell senescence in mediating either lung fibrosis or lung emphysema is further illustrated by reports of lung fibrosis, lung emphysema, or both in individuals carrying a mutation in the telomerase *TERT* gene [14, 34]. The mechanisms that may favor development of lung emphysema, lung fibrosis, or both in response to cell senescence, still remain unclarified although it is likely that different senescent cell types drive these different phenotypes. Consistent with this, we found that mice injected intratracheally with a lentiviral vector encoding *PLA2R1* rapidly developed severe lung emphysema and some degree of pulmonary hypertension, but without significant lung fibrosis. It is therefore possible that the relatively small number of transduced cells, although sufficient to induce lung emphysema, was probably insufficient to induce lung fibrosis as seen with PLA2R1-TG mice.

In the PLA2R1- TG mouse model, short-term ruxolitinib treatment markedly diminished the lung fibrotic and emphysema lesions, the lung p16 levels, SASP members, and JAK/STAT downstream gene expression. Moreover, in mice injected intratracheally with the LV-*PLA2R1* vector, ruxolitinib treatment started at the time of lentiviral administration prevented lung-cell senescence and lung emphysema development. These results are consistent with an inhibitory effect of ruxolitinib on PLA2R1-induced lung-cell senescence, either by a direct effect or by an effect mediated by inhibition of the SASP. Inhibitors of the JAK/STAT pathways may have complex actions since they have also been

shown to inhibit TGF-β signaling in lung cells. Our results therefore do not allow to draw definitive conclusions about the mechanism of action of ruxolitinib, and further studies are needed to assess the potential protective effects of this drug on lung alterations in other models.

Taken together, our findings support a causal role for *PLA2R1* activation-induced cell senescence in lung pathology and support the view that targeting the PLA2R1-JAK2 pathway represents a therapeutic option for inhibiting cell senescence or eliminating the SASP in patients with COPD. In contrast to interventions targeting major senescence pathways such as the p53 pathway, targeting PLA2R1 and/or the JAK pathway should not drastically impact tumor development. Anti-JAK agents are currently used to treat cancer and were recently found to reprogram the SASP in senescent tumor cells, an effect that contributes to improve their antitumor effect. Further studies are needed to evaluate the potential of this approach as a new therapeutic option in COPD.

Acknowledgments

We are grateful to A Lalot, D Gelperowic, A Ribeiro Da Silva, A Da Silva and F Weber from the Plateforme de Physiologie et Physiopathologie Expérimentale, as well as to X. Decrouy, and C. Micheli from the imaging platform facility; IMRB Inserm, Créteil, France. Thomas Lilin, Centre de recherche Biomédicale d'Alfort (CRBM), National veterinary school of Alfort.

Authors' contributions

D.B..: conception and design, acquisition, analysis and interpretation of data, and drafting of manuscript; A.A.: conception and design, acquisition, analysis and interpretation of data, and drafting of manuscript; M.B.: acquisition, analysis and interpretation of data; L.L.: conception and design, acquisition, analysis and interpretation of data; E.M.: acquisition, analysis and interpretation of data; E.B.: acquisition, analysis and interpretation of data; J.H.: acquisition, analysis and interpretation of data; S.Ab.: conception and design, acquisition, analysis and interpretation of data, and drafting of manuscript; A.H.: acquisition, analysis and interpretation of data; G.D.: analysis and interpretation of data, and revising of manuscript; B.M.: analysis and interpretation of data, and revising of manuscript; M.L.: analysis and interpretation of data and revising of manuscript; N.V.: acquisition, analysis and interpretation of data; P.B.: acquisition, analysis and interpretation of data; S.J.: acquisition, analysis and interpretation of data; H.N.: analysis and interpretation of data, revising manuscript; D.G.: acquisition, analysis and interpretation of data; D.V.: acquisition, analysis and interpretation of data; D. Bernard.: conception and design, analysis and interpretation of data, and revising of manuscript; S.A.: conception and design, analysis and interpretation of data, and drafting of manuscript.

Funding: This study was supported by grants from the INSERM, *Délégation à la Recherche Clinique de l'AP-HP - FHU SENEC, Fondation pour la Recherche Médicale* (*FRM*), *Legs Poix, Agence Nationale pour la Recherche* (*ANR*) *and Institut National Du Cancer (INCA).*

Data availability

The data that support the findings of this study are available from the corresponding author upon request.

References

1. Childs BG, Gluscevic M, Baker DJ, Laberge RM, Marquess D, Dananberg J, van Deursen JM. Senescent cells: an emerging target for diseases of ageing. *Nat Rev Drug Discov* 2017.

2. Gershon AS, Warner L, Cascagnette P, Victor JC, To T. Lifetime risk of developing chronic obstructive pulmonary disease: a longitudinal population study. *Lancet* 2011: 378(9795): 991-996.

3. Han MK, Agusti A, Calverley PM, Celli BR, Criner G, Curtis JL, Fabbri LM, Goldin JG, Jones PW, Macnee W, Make BJ, Rabe KF, Rennard SI, Sciurba FC, Silverman EK, Vestbo J, Washko GR, Wouters EF, Martinez FJ. Chronic obstructive pulmonary disease phenotypes: the future of COPD. *Am J Respir Crit Care Med* 2010: 182(5): 598-604.

4. Adnot S, Amsellem V, Boyer L, Marcos E, Saker M, Houssaini A, Kebe K, Dagouassat M, Lipskaia L, Boczkowski J. Telomere Dysfunction and Cell Senescence in Chronic Lung Diseases: Therapeutic Potential. *Pharmacol Ther* 2015: 153: 125-134.

5. Vanfleteren LE, Spruit MA, Groenen M, Gaffron S, van Empel VP, Bruijnzeel PL, Rutten EP, Op 't Roodt J, Wouters EF, Franssen FM. Clusters of comorbidities based on validated objective measurements and systemic inflammation in patients with chronic obstructive pulmonary disease. *Am J Respir Crit Care Med* 2013: 187(7): 728-735.

6. Amsellem V, Gary-Bobo G, Marcos E, Maitre B, Chaar V, Validire P, Stern JB, Noureddine H, Sapin E, Rideau D, Hue S, Le Corvoisier P, Le Gouvello S, Dubois-Rande JL, Boczkowski J, Adnot S. Telomere dysfunction causes sustained inflammation in chronic obstructive pulmonary disease. *Am J Respir Crit Care Med* 2011: 184(12): 1358-1366.

7. Houssaini A, Breau M, Kebe K, Abid S, Marcos E, Lipskaia L, Rideau D, Parpaleix A, Huang J, Amsellem V, Vienney N, Validire P, Maitre B, Attwe A, Lukas C, Vindrieux D,

Boczkowski J, Derumeaux G, Pende M, Bernard D, Meiners S, Adnot S. mTOR pathway activation drives lung cell senescence and emphysema. *JCI Insight* 2018: 3(3).

8. Savale L, Chaouat A, Bastuji-Garin S, Marcos E, Boyer L, Maitre B, Sarni M, Housset B, Weitzenblum E, Matrat M, Le Corvoisier P, Rideau D, Boczkowski J, Dubois-Rande JL, Chouaid C, Adnot S. Shortened telomeres in circulating leukocytes of patients with chronic obstructive pulmonary disease. *Am J Respir Crit Care Med* 2009: 179(7): 566-571.

9. Tsuji T, Aoshiba K, Nagai A. Cigarette smoke induces senescence in alveolar epithelial cells. *Am J Respir Cell Mol Biol* 2004: 31(6): 643-649.

10. Freund A, Orjalo AV, Desprez PY, Campisi J. Inflammatory networks during cellular senescence: causes and consequences. *Trends Mol Med* 2010: 16(5): 238-246.

11. Munoz-Espin D, Serrano M. Cellular senescence: from physiology to pathology. *Nat Rev Mol Cell Biol* 2014: 15(7): 482-496.

12. Armanios M, Blackburn EH. The telomere syndromes. *Nat Rev Genet* 2012: 13(10): 693-704.

13. Andujar P, Courbon D, Bizard E, Marcos E, Adnot S, Boyer L, Demoly P, Jarvis D, Neukirch C, Pin I, Thabut G, Boczkowski J, Leynaert B. Smoking, telomere length and lung function decline: a longitudinal population-based study. *Thorax* 2018: 73(3): 283-285.

14. Alder JK, Guo N, Kembou F, Parry EM, Anderson CJ, Gorgy AI, Walsh MF, Sussan T, Biswal S, Mitzner W, Tuder RM, Armanios M. Telomere length is a determinant of emphysema susceptibility. *Am J Respir Crit Care Med* 2011: 184(8): 904-912.

15. Yao H, Chung S, Hwang JW, Rajendrasozhan S, Sundar IK, Dean DA, McBurney MW, Guarente L, Gu W, Ronty M, Kinnula VL, Rahman I. SIRT1 protects against emphysema via FOXO3-mediated reduction of premature senescence in mice. *J Clin Invest* 2012: 122(6): 2032-2045.

16. Augert A, Payre C, de Launoit Y, Gil J, Lambeau G, Bernard D. The M-type receptor PLA2R regulates senescence through the p53 pathway. *EMBO Rep* 2009: 10(3): 271-277.

17. Ancian P, Lambeau G, Lazdunski M. Multifunctional activity of the extracellular domain of the M-type (180 kDa) membrane receptor for secretory phospholipases A2. *Biochemistry* 1995: 34(40): 13146-13151.

18. Augert A, Vindrieux D, Girard CA, Le Calve B, Gras B, Ferrand M, Bouchet BP, Puisieux A, de Launoit Y, Simonnet H, Lambeau G, Bernard D. PLA2R1 kills cancer cells by inducing mitochondrial stress. *Free Radic Biol Med* 2013: 65: 969-977.

19. Vindrieux D, Augert A, Girard CA, Gitenay D, Lallet-Daher H, Wiel C, Le Calve B, Gras B, Ferrand M, Verbeke S, de Launoit Y, Leroy X, Puisieux A, Aubert S, Perrais M, Gelb M, Simonnet H, Lambeau G, Bernard D. PLA2R1 mediates tumor suppression by activating JAK2. *Cancer Res* 2013: 73(20): 6334-6345.

20. Bernard D, Vindrieux D. PLA2R1: expression and function in cancer. *Biochim Biophys Acta* 2014: 1846(1): 40-44.

21. Griveau A, Devailly G, Eberst L, Navaratnam N, Le Calve B, Ferrand M, Faull P, Augert A, Dante R, Vanacker JM, Vindrieux D, Bernard D. The PLA2R1-JAK2 pathway upregulates ERRalpha and its mitochondrial program to exert tumor-suppressive action. *Oncogene* 2016: 35(38): 5033-5042.

22. Griveau A, Wiel C, Le Calve B, Ziegler DV, Djebali S, Warnier M, Martin N, Marvel J, Vindrieux D, Bergo MO, Bernard D. Targeting the phospholipase A2 receptor ameliorates premature aging phenotypes. *Aging Cell* 2018: 17(6): e12835.

23. Griveau A, Wiel C, Ziegler DV, Bergo MO, Bernard D. The JAK1/2 inhibitor ruxolitinib delays premature aging phenotypes. *Aging Cell* 2020: 19(4): e13122.

24. Murakami M, Lambeau G. Emerging roles of secreted phospholipase A(2) enzymes: an update. *Biochimie* 2013: 95(1): 43-50.

25. Childs BG, Baker DJ, Wijshake T, Conover CA, Campisi J, van Deursen JM. Senescent intimal foam cells are deleterious at all stages of atherosclerosis. *Science* 2016: 354(6311): 472-477.

26. Adcock IM, Mumby S, Caramori G. Breaking news: DNA damage and repair pathways in COPD and implications for pathogenesis and treatment. *Eur Respir J* 2018: 52(4).

27. Noureddine H, Gary-Bobo G, Alifano M, Marcos E, Saker M, Vienney N, Amsellem V, Maitre B, Chaouat A, Chouaid C, Dubois-Rande JL, Damotte D, Adnot S. Pulmonary artery smooth muscle cell senescence is a pathogenic mechanism for pulmonary hypertension in chronic lung disease. *Circ Res* 2011: 109(5): 543-553.

28. Yew-Booth L, Birrell MA, Lau MS, Baker K, Jones V, Kilty I, Belvisi MG. JAK-STAT pathway activation in COPD. *Eur Respir J* 2015: 46(3): 843-845.

29. Xu M, Tchkonia T, Ding H, Ogrodnik M, Lubbers ER, Pirtskhalava T, White TA, Johnson KO, Stout MB, Mezera V, Giorgadze N, Jensen MD, LeBrasseur NK, Kirkland JL. JAK inhibition alleviates the cellular senescence-associated secretory phenotype and frailty in old age. *Proc Natl Acad Sci U S A* 2015: 112(46): E6301-6310.

30. Seimetz M, Parajuli N, Pichl A, Veit F, Kwapiszewska G, Weisel FC, Milger K, Egemnazarov B, Turowska A, Fuchs B, Nikam S, Roth M, Sydykov A, Medebach T, Klepetko W, Jaksch P, Dumitrascu R, Garn H, Voswinckel R, Kostin S, Seeger W, Schermuly RT, Grimminger F, Ghofrani HA, Weissmann N. Inducible NOS inhibition reverses tobacco-smoke-induced emphysema and pulmonary hypertension in mice. *Cell* 2011: 147(2): 293-305.

31. Schafer MJ, White TA, Iijima K, Haak AJ, Ligresti G, Atkinson EJ, Oberg AL, Birch J, Salmonowicz H, Zhu Y, Mazula DL, Brooks RW, Fuhrmann-Stroissnigg H, Pirtskhalava T, Prakash YS, Tchkonia T, Robbins PD, Aubry MC, Passos JF, Kirkland JL, Tschumperlin

DJ, Kita H, LeBrasseur NK. Cellular senescence mediates fibrotic pulmonary disease. *Nat Commun* 2017: 8: 14532.

32. Jiang C, Liu G, Luckhardt T, Antony V, Zhou Y, Carter AB, Thannickal VJ, Liu RM. Serpine 1 induces alveolar type II cell senescence through activating p53-p21-Rb pathway in fibrotic lung disease. *Aging Cell* 2017: 16(5): 1114-1124.

33. Barkauskas CE, Noble PW. Cellular mechanisms of tissue fibrosis. 7. New insights into the cellular mechanisms of pulmonary fibrosis. *Am J Physiol Cell Physiol* 2014: 306(11): C987-996.

34. Stanley SE, Chen JJ, Podlevsky JD, Alder JK, Hansel NN, Mathias RA, Qi X, Rafaels NM, Wise RA, Silverman EK, Barnes KC, Armanios M. Telomerase mutations in smokers with severe emphysema. *J Clin Invest* 2014: 125(2): 563-570.

Figure legends

Figure 1: Analysis of lung samples from patients with COPD and controls. (a) Protein levels of PLA2R1, p21 and p16 measured in the lungs of 23 patients with COPD and 23 controls. Graphs represent individual values with the mean; representative immunoblots are shown on the right. *P<0.05, **P<0.01 compared with values from controls by two-tailed unpaired Student's t test. (b) From left to right, representative micrographs of lung tissue from patients with COPD and controls showing immunofluorescence of PLA2R1 (white) in endothelial cells identified by CD31 (red), pulmonary artery smooth muscle cells identified by α-SMA (red), and alveolar type II cells identified by MUC1 (red). Elastin autofluorescence (green). Nuclei were labeled with DAPI (blue). (c) Representative micrographs of PLA2R1-positive vascular cells and alveolar epithelial type II cells also stained for p16.

Figure 2: Co-localization of PLA2R1 and DNA damage markers in lung from patients with COPD and controls. (a) Representative micrographs of PLA2R1-positive alveolar epithelial type II cells (left panel) and vascular cells (right panel) also stained for 53BP1 (red). (b) Similar representation showing PLA2R1-positive cells also stained for p-gH2AX (red). The zoom areas are indicated by squares.

Figure 3: Analysis of primary PA-SMCs (a) and P-ECs (b) isolated from pulmonary arteries of patients with COPD and controls. From left to right, cumulative PDL, percentage of β-Gal-positive cells, and *PLA2R1* mRNA levels shown at the corresponding cell passage in cultured (a) PA-SMCs (n=7 in each group) and (b) P-ECs (n=8 in each group) from patients with COPD and controls. Values are means±SEM or individual values

with the mean. *P<0.05, ***P<0.001 vs. control cells, two-way ANOVA with Bonferroni's multiple comparisons test. Representative photographs of cultured β-Gal-stained PA-SMCs (a) and P-ECs (b) at the indicated cell passages.

Figure 4: Effect of *PLA2R1* knockdown on senescence of PA-SMCs from patients with COPD and controls. Cells were infected with a retroviral vector encoding an shRNA that targeted *PLA2R1* (sh*PLA2R1*) or with a control vector (shControl) then subjected to successive cell passages. (a) Graphs showing the mean±SEM of PDL at successive cell passages of PA-SMCs from 10 controls and 6 patients with COPD. PDLs at passage 6 are shown as individual values with the mean. (b) Graph showing the percentage of β-Gal-positive cells at passage 6, with representative photographs of β-Gal stained cells. (c) Graphs showing the cell protein levels of p16 and p21 (individual values with the mean) with representative immunoblots in PA-SMCs from 7 controls and 5 COPD patients at passage 6. a, b, c, **P<0.01, ***P<0.001, two-way ANOVA with Bonferroni's multiple comparisons test (d) Protein levels of IL-8, IL-6, and PAI-1 in PA-SMC-conditioned media at passage 6. Data are shown as median (interquartile range) of 5 (COPD patients) to 10 (controls) values per group. Bars represent extreme values. *P<0.05, Kruskal-Wallis and Dunn tests.

Figure 5: Effect of ectopic *PLA2R1* expression on senescence of PA-SMCs treated with the JAK1/2 inhibitor ruxolitinib or its vehicle. PA-SMCs were infected with a retrovirus encoding the human *PLA2R1* gene (*PLA2R1* virus) or with a control vector then subjected to successive passages in the presence of ruxolitinib (0.5 µM) or its vehicle. (a) Representative micrographs of cells co-stained for PLA2R1 (red) and for phosphorylated JAK2 (p-JAK2) or STAT3 (p-STAT3) (green). (b) Cells stained for PLA2R1 (red) were positive for p16 and negative for PCNA (yellow) when treated with the vehicle but not when treated with

ruxolitinib. (c) Graphs showing the mean±SEM of cumulative PDLs of cells infected with the Control vector or with the *PLA2R1* virus and treated with vehicle or ruxolitinib (0.5µM) n=5 in each group. Graph showing the percentage of β-Gal-positive cells at passage 8, with representative photographs of β-Gal stained cells (right panel). $^{\#}P<0.05$, $^{\#\#}P<0.01$ comparaison values from vehicle vs ruxolitinib, $*P<0.05$, $**P<0.01$ comparaison values from Control vector vs PLA2R1 virus, one-tailed Student's paired *t*-test. (d) Protein levels of IL-8, IL-6, and PAI-1 in conditioned media from the indicated cultures at passage 8. Data are shown as median (interquartile range) of 5 values per group. Bars represent extreme values. $*P<0.05$, Kruskal-Wallis followed by Wilcoxon test.

Figure 6: Effects of treatment with ruxolitinib on senescence of cultured PA-SMCs from patients with COPD and controls. (a) Representative micrographs of lung tissue from patients with COPD and controls showing immunofluorescent of JAK2 (red) and PLA2R1 (white) in pulmonary vessels and alveoli. Elastin autofluorescence (green). Nuclei were labeled with DAPI (blue). (b) Representative micrographs showing phospho-STAT3 positive cells (brown) in vessels and alveoli. (c) Effect of continuous ruxolitinib treatment on senescence of PA-SMCs from patients with COPD (n=8) and controls (n=5) as assessed by the number of PDLs and the percentage of β-Gal-positive cells at passage 6. Typical cells stained for β-Gal are shown on the right. $*P<0.05$, $**P<0.01$, $***P<0.001$, two-way ANOVA with Bonferroni's multiple comparisons test. (d) Protein levels of IL-8, IL-6, and PAI-1 in conditioned media of cells from patients with COPD and controls treated with ruxolitinib or its vehicle. Data are shown as the median (interquartile range) of 5 values per group. Bars represent extreme values. $**P<0.01$, $***P<0.001$ compared with control, two-tailed Mann Whitney test.

Figure 7: Lung characteristics of transgenic mice constitutively expressing the human *PLA2R1* gene (*PLA2R1*-TG) and their littermates (NTG) subjected to 15 days of ruxolitinib treatment. (a) Lung protein levels of PLA2R1 and p16 in *PLA2R1*-TG (n=16) and NTG (n=15) mice treated with ruxolitinib (75 mg/kg/day) or its vehicle, with their representative immunoblots below. Representative micrographs of lung tissue from *PLA2R1*-TG and NTG showing co-localization of PLA2R1 (white) and p16 (red) in pulmonary vessels and alveoli shown on the right (b) Lung mRNA levels of the JAK2 signaling target genes Tap1, Socs1, and Irf7 in each condition. (c) Lung emphysema as assessed by measurement of the mean linear intercept (MLI) and (d) lung fibrosis as assessed by the modified Ashcroft score. Representative images of lungs from the four groups of mice stained with Masson's trichrome (top and middle panels, in blue) and with Sirius Red (bottom panel, in red). (e) Lung mRNA levels of collagens 1A1 and A2 (Col1A1, Col1A2), collagen 3A1 (Col3A1), actin alpha 2 (ACTA2), and fibronectin and (f) lung protein levels of IL-6,, MCP-1, IL-1β and PAI-1. **P*<0.05, ***P*<0.01 ****P*<0.001. Two-way ANOVA with Bonferroni's multiple comparisons test.

Figure 8: Lung characteristics of mice subjected to intratracheal injection of a lentivirus encoding murine *Pla2r1* gene (LV-*PLA2R1*) and concomitantly treated with ruxolitinib. Mice treated with the LV-*PLA2R1* or a control vector (LV-ncRNA) and simultaneously treated with ruxolitinib (75 mg/kg/day) or vehicle were studied 30 days after the injection. (a) Representative micrographs showing *PLA2R1* immunofluorescence (red) in mouse lung sections. (b) Lung mRNA levels of *PLA2R1* and of the JAK2 signaling target genes Tap1, Socs1, and Irf7. (c) Lung protein levels of p21 and p16 with representative immunoblots in the indicated groups (d) Lung emphysema as assessed by measurement of the mean linear intercept (MLI) in hematoxylin and eosin-stained lung sections. **P*<0.05,

**P<0.01 ***P<0.001. Student's *t*-test; two-way ANOVA with Bonferroni's multiple comparisons test.

Online supplementary figures

Supplemental Figure 1: Distribution of PLA2R1 immunofluorescence activity in lungs from patients with COPD and controls. Representative micrographs of lung tissue from 3 patients with COPD and 3 controls showing PLA2R1 expression (white), and merge with elastin autofluorescence (green) and nuclear DAPI staining (blue). The zoom area is indicated by a square.

Supplemental Figure 2: *PLA2R1* mRNA levels measured in cells stably infected with the sh*PLA2R1*-encoding retroviral vector, compared to cells infected with the control vector. ***P<0.001 for comparison between groups, Student's *t*-test

Supplemental Figure 3: Comparison between inactivation of *PLA2R1* and *p53* in cells from patients with COPD and controls. Cells from patients with COPD (n=5) and controls (n=5) were infected either with a retroviral vector encoding an shRNA that targeted *PLA2R1* (sh*PLA2R1*) or *p53* (sh*p53*) or with a control vector encoding a scramble sequence (shControl). The cells were then subjected to successive passages. (a, b) Graphs showing cumulative numbers of PDLs, percentage of β-Gal-positive cells, and p16 and p21 protein levels as assessed by Western blotting, all determined at passage 6 are shown as individual values with the mean. Representative immunoblots are shown on the right. *P<0.05, **P<0.01, ***P<0.001 vs. shControl, two-way ANOVA with Bonferroni's multiple

comparisons test. (c) Protein levels of IL-8, IL-6, and PAI-1 in PA-SMC-conditioned media at passage 6. Data are shown as median (interquartile range) of 5 values per group. Bars represent extreme values. There were no significant differences between values recorded in cells treated with the sh*PLA2R1* or the sh*p53* vectors. **P*<0.05, ***P*<0.01 vs. shControl one-tailed Mann Whitney test.

Supplemental Figure 4: Lung vimentin and fibroblast-specific protein (FSP) immunostaining in *PLA2R1*TG mice and littermate controls subjected to 15 days of treatment with ruxolitinib or vehicle. (a) Representative micrographs showing lung sections stained for vimentin (red), a lung alveolar fibroblast

t marker, in *PLA2R1*-TG and control mice treated with ruxolitinib or vehicle. Elastin autofluorescence (green); the nuclei were stained with DAPI (blue). (b) Representative micrographs showing lung sections stained for fibroblast-specific protein (FSP, brown), a lung alveolar fibroblast marker, in the same groups of mice.

Supplemental Figure 5: Pulmonary hemodynamic parameters in *PLA2R1*TG and littermate control (NTG) mice subjected to 15 days of treatment with ruxolitinib or vehicle. (a) Right ventricular systolic pressure (RVSP) (b) Right ventricular hypertrophy index (Fulton's index) (c) Muscularization of pulmonary vessels (percent of muscularized vessels over the total number of pulmonary vessels) and representative images of pulmonary vessels. Graphs represent individual values with the mean±SEM. ***P*<0.01, ****P*<0.001 for comparisons between groups as indicated. Unpaired Student's *t*-test and two-way ANOVA with Bonferroni's multiple comparisons test.

Supplemental figure 6. Identification of lentivirus-transduced cells in the mouse lung.

A lentiviral vector encoding the mCherry gene under the control of the CMV promoter (LV-mCherry) was injected intratracheally to mice (109 TU/ml diluted in DPBS with 5% of Lipofectamine 2000) in comparison with vehicle (DPBS with 5% of Lipofectamine 2000). , Mice were sacrificed on day 9 post-infection, and lung cryosections were assessed by fluorescence microscopy for mCherry reporter gene expression. Green – elastin autofluorescence, nuclei were stained with DAPI (blue). Bar – 50µm.

Supplemental Figure 7: Pulmonary hemodynamic parameters in mice subjected to an intratracheal injection of a lentivirus encoding the mouse *Pla2r1* gene (LV-*PLA2R1*) and concomitantly treated with ruxolitinib. Mice treated with the LV-*PLA2R1* or a control vector (LV-ncRNA) and simultaneously treated with ruxolitinib (75 mg/kg/day) or vehicle were studied 30 days after the injection. (a) Lung mRNA level of p21 (b) Right ventricular systolic pressure (RVSP) (c) Right ventricular hypertrophy index (Fulton's index) (d) Muscularization of pulmonary vessels (percent of muscularized vessels over the total number of pulmonary vessels) and representative images of pulmonary vessels. Graphs represent individual values with the mean±SEM. $^{**}P<0.01$, $^{***}P<0.001$ for comparisons between groups as indicated. Student's *t*-test and two-way ANOVA with Bonferroni's multiple comparisons test.

Supplementary Tables

Supplemental Tables S1 and S2: Clinical features and pathological variables of patients with COPD and control smokers. Table S1 describes all patients and controls from whom

lung samples were obtained. Cells were collected from a subset of 8 patients and 10 controls, whose characteristics are described in Table S2.

Abbreviations: FEV_1, forced expiratory volume in 1 second; FEV_1%, percentage of the predicted FEV_1 value; FVC, forced vital capacity; FVC%, percentage of the predicted FVC value.

Supplemental Table S3: TaqMan Gene Expression assays

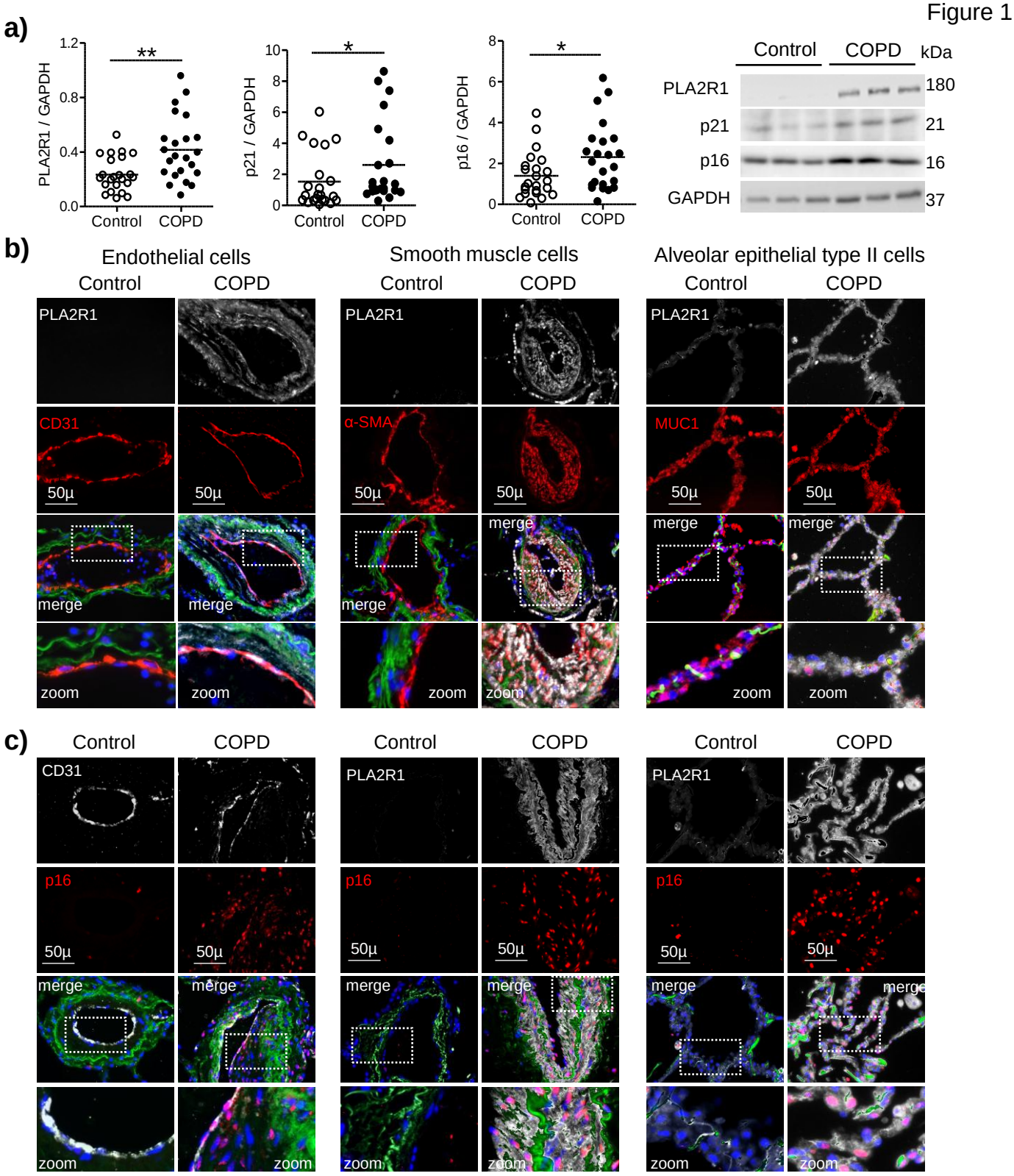

Figure 1: Analysis of lung samples from patients with COPD and controls

(a) Protein levels of PLA2R1, p21 and p16 measured in the lungs of 23 patients with COPD and 23 controls. Graphs represent individual values with the mean; representative immunoblots are shown on the right. **P*<0.05, ***P*<0.01 compared with values from controls by two-tailed unpaired Student's *t* test. **(b)** From left to right, representative micrographs of lung tissue from patients with COPD and controls showing immunofluorescence of *PLA2R1* (white) in endothelial cells identified by CD31 (red), pulmonary artery smooth muscle cells identified by α-SMA (red), and alveolar type II cells identified by MUC1 (red). Elastin autofluorescence (green). Nuclei were labeled with DAPI (blue). **(c)** Representative micrographs of PLA2R1-positive vascular cells and alveolar epithelial type II cells also stained for p16.

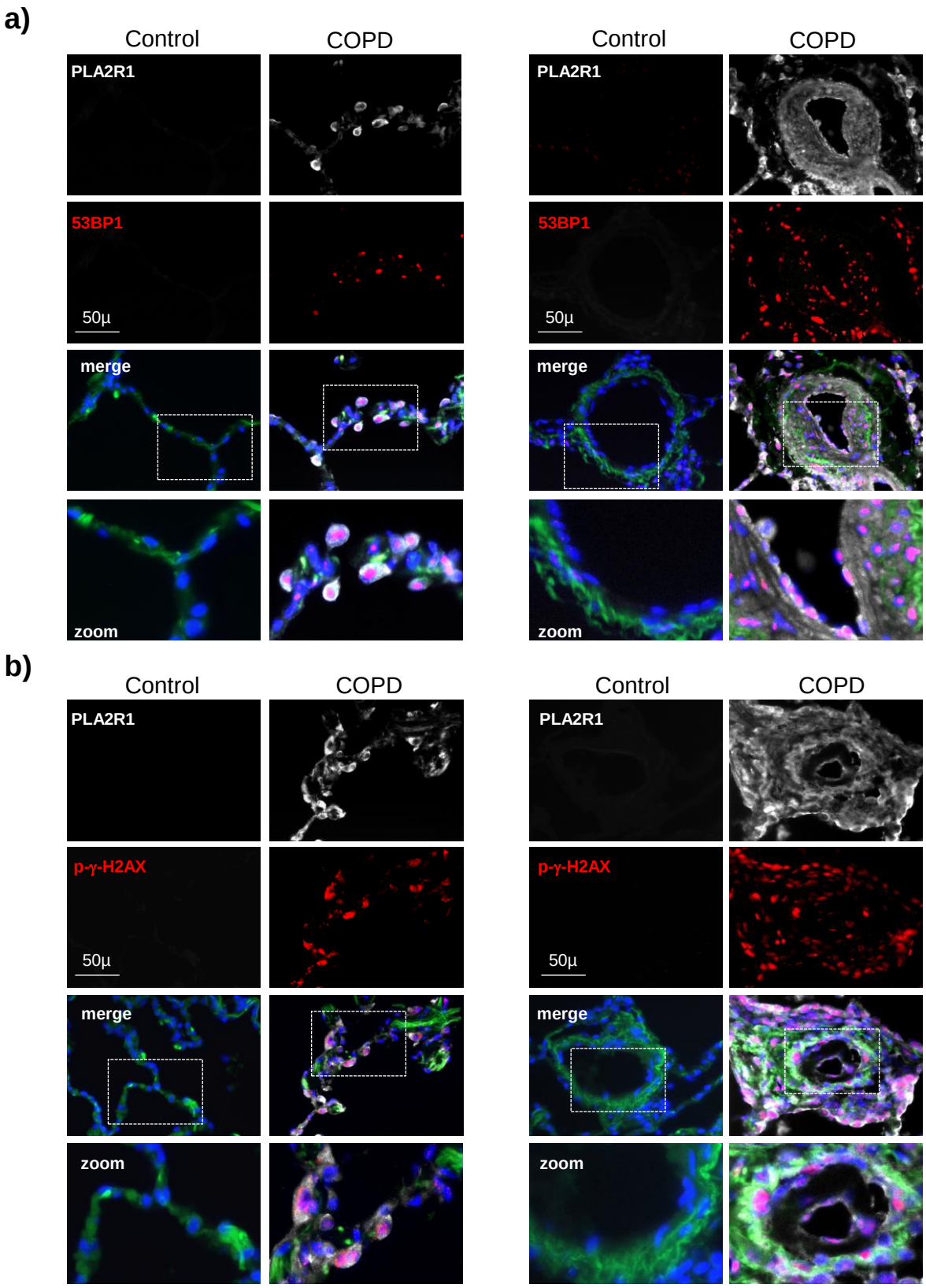

Figure 2. Co-localization of PLA2R1 and DNA damage markers in lung from patients with COPD and controls
(a) Representative micrographs of PLA2R1-positive alveolar epithelial type II cells (left panel) and vascular cells (right panel) also stained for 53BP1 (red). **(b)** Similar representation showing PLA2R1-positive cells also stained for p-γH2AX (red). The zoom areas are indicated by squares.

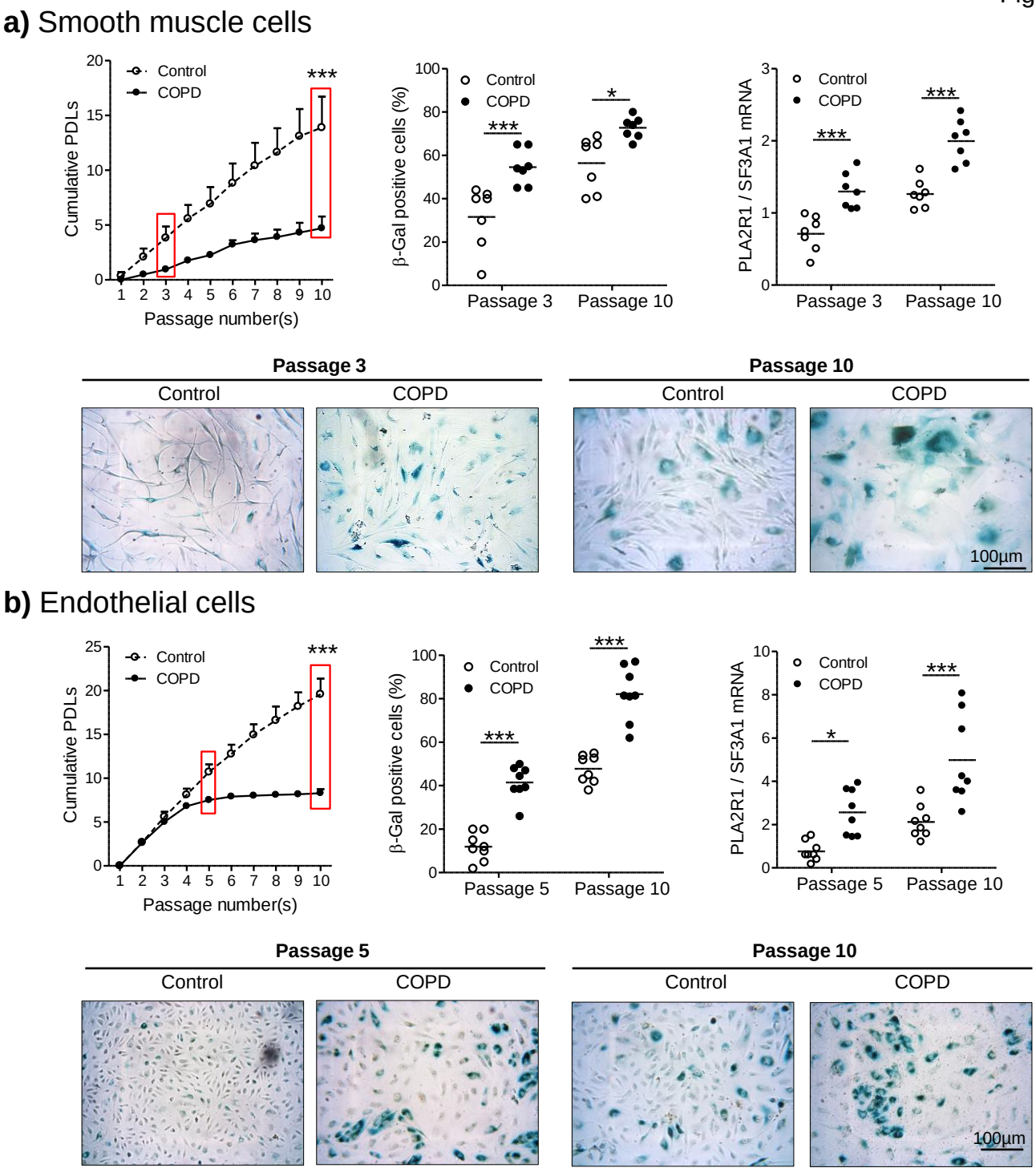

Figure 3: Analysis of primary PA-SMCs (a) and P-ECs (b) isolated from pulmonary arteries of patients with COPD and controls

From left to right, cumulative PDL, percentage of β-Gal-positive cells, and *PLA2R1* mRNA levels shown at the corresponding cell passage in cultured **(a)** PA-SMCs (n=7 in each group) and **(b)** P-ECs (n=8 in each group) from patients with COPD and controls. Values are means±SEM or individual values with the mean. **P*<0.05, ****P*<0.001 vs. control cells, two-way ANOVA with Bonferroni's multiple comparisons test. Representative photographs of cultured β-Gal-stained PA-SMCs (a) and P-ECs (b) at the indicated cell passages.

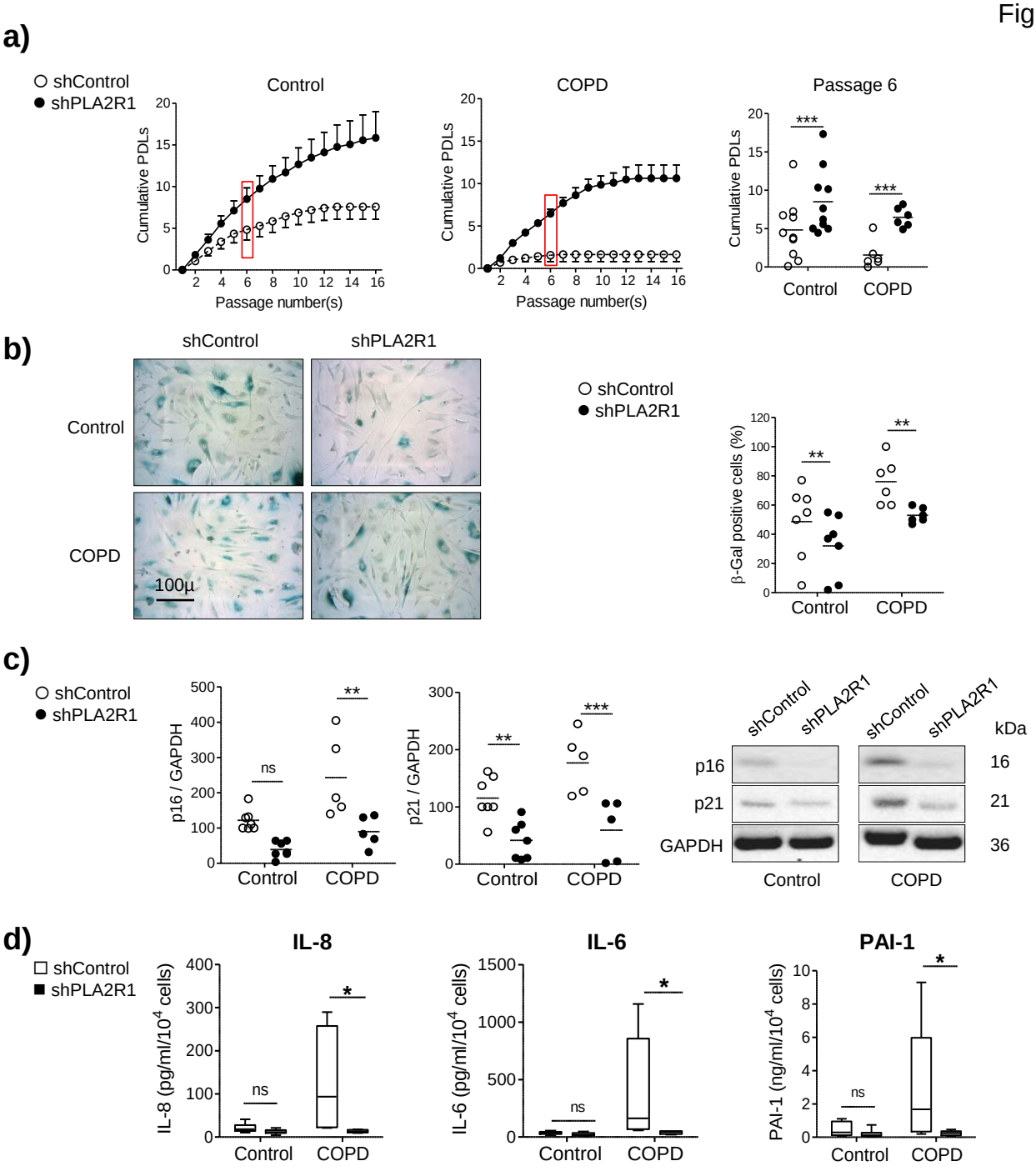

Figure 4: Effect of *PLA2R1* knockdown on senescence of PA-SMCs from patients with COPD and controls
Cells were infected with a retroviral vector encoding an shRNA that targeted *PLA2R1* (sh*PLA2R1*) or with a control vector (shControl) then subjected to successive cell passages. **(a)** Graphs showing the mean±SEM of PDL at successive cell passages of PA-SMCs from 10 controls and 6 patients with COPD. PDLs at passage 6 are shown as individual values with the mean. **(b)** Graph showing the percentage of β-Gal-positive cells at passage 6, with representative photographs of β-Gal stained cells. **(c)** Graphs showing the cell protein levels of p16 and p21 (individual values with the mean) with representative immunoblots in PA-SMCs from 7 controls and 5 COPD patients at passage 6. **a, b, c**, ***P*<0.01, ****P*<0.001, two-way ANOVA with Bonferroni's multiple comparisons test **(d)** Protein levels of IL-8, IL-6, and PAI-1 in PA-SMC-conditioned media at passage 6. Data are shown as median (interquartile range) of 5 (COPD patients) to 10 (controls) values per group. Bars represent extreme values. **P*<0.05, Kruskal-Wallis and Dunn tests.

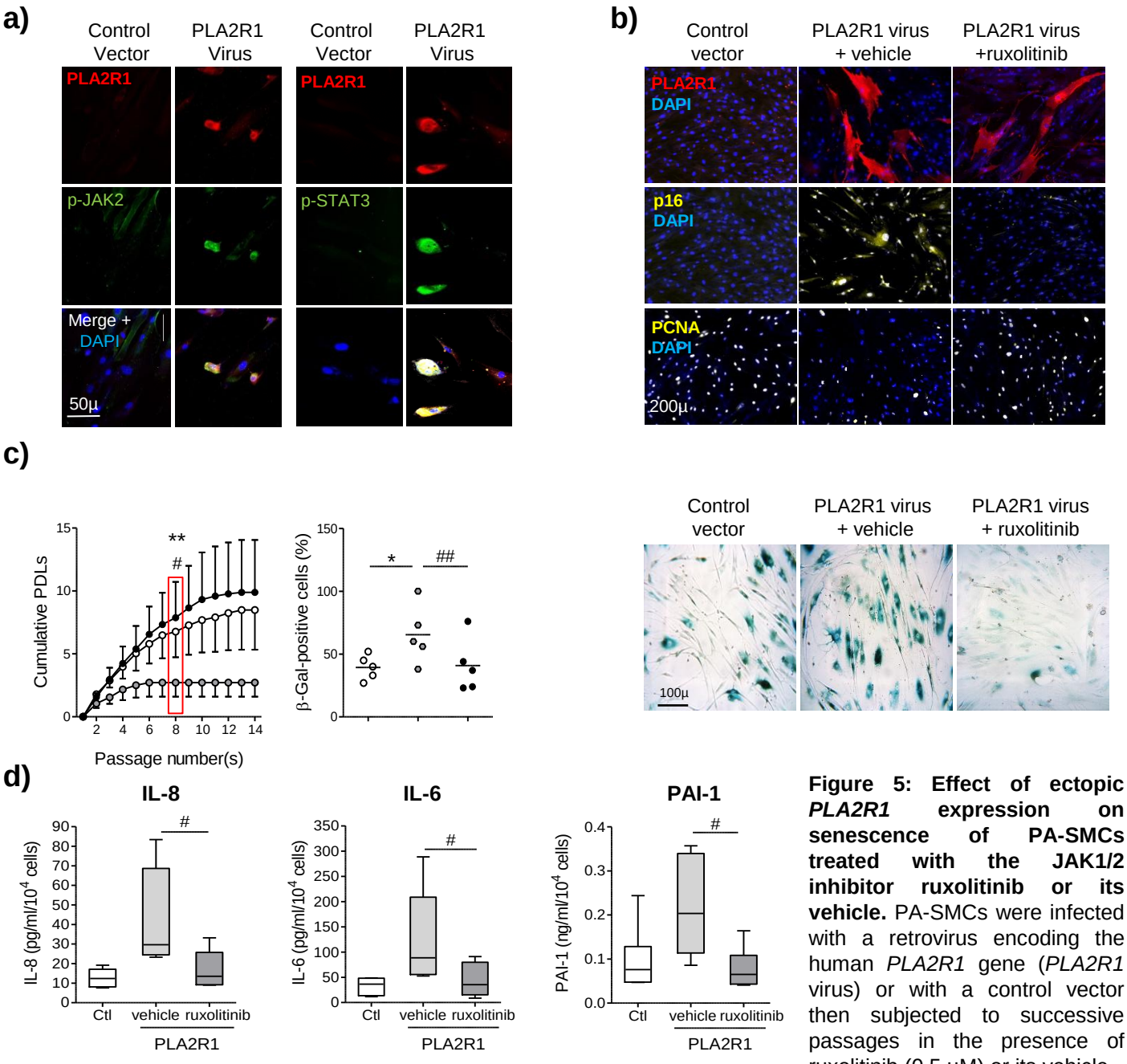

Figure 5: Effect of ectopic *PLA2R1* expression on senescence of PA-SMCs treated with the JAK1/2 inhibitor ruxolitinib or its vehicle. PA-SMCs were infected with a retrovirus encoding the human *PLA2R1* gene (*PLA2R1* virus) or with a control vector then subjected to successive passages in the presence of ruxolitinib (0.5 µM) or its vehicle.

(a) Representative micrographs of cells co-stained for PLA2R1 (red) and for phosphorylated JAK2 (p-JAK2) or STAT3 (p-STAT3) (green). **(b)** Cells stained for PLA2R1 (red) were positive for p16 and negative for PCNA (yellow) when treated with the vehicle but not when treated with ruxolitinib. **(c)** Graphs showing the mean±SEM of cumulative PDLs of cells infected with the Control vector or with the *PLA2R1* virus and treated with vehicle or ruxolitinib (0.5µM) n=5 in each group. Graph showing the percentage of β-Gal-positive cells at passage 8, with representative photographs of β-Gal stained cells (right panel). $^{\#}P<0.05$, $^{\#\#}P<0.01$ comparaison values from vehicle vs ruxolitinib, $^{*}P<0.05$, $^{**}P<0.01$ comparaison values from Control vector vs PLA2R1 virus, one-tailed Student's paired *t*-test. **(d)** Protein levels of IL-8, IL-6, and PAI-1 in conditioned media from the indicated cultures at passage 8. Data are shown as median (interquartile range) of 5 values per group. Bars represent extreme values. $^{*}P<0.05$, Kruskal-Wallis followed by Wilcoxon test.

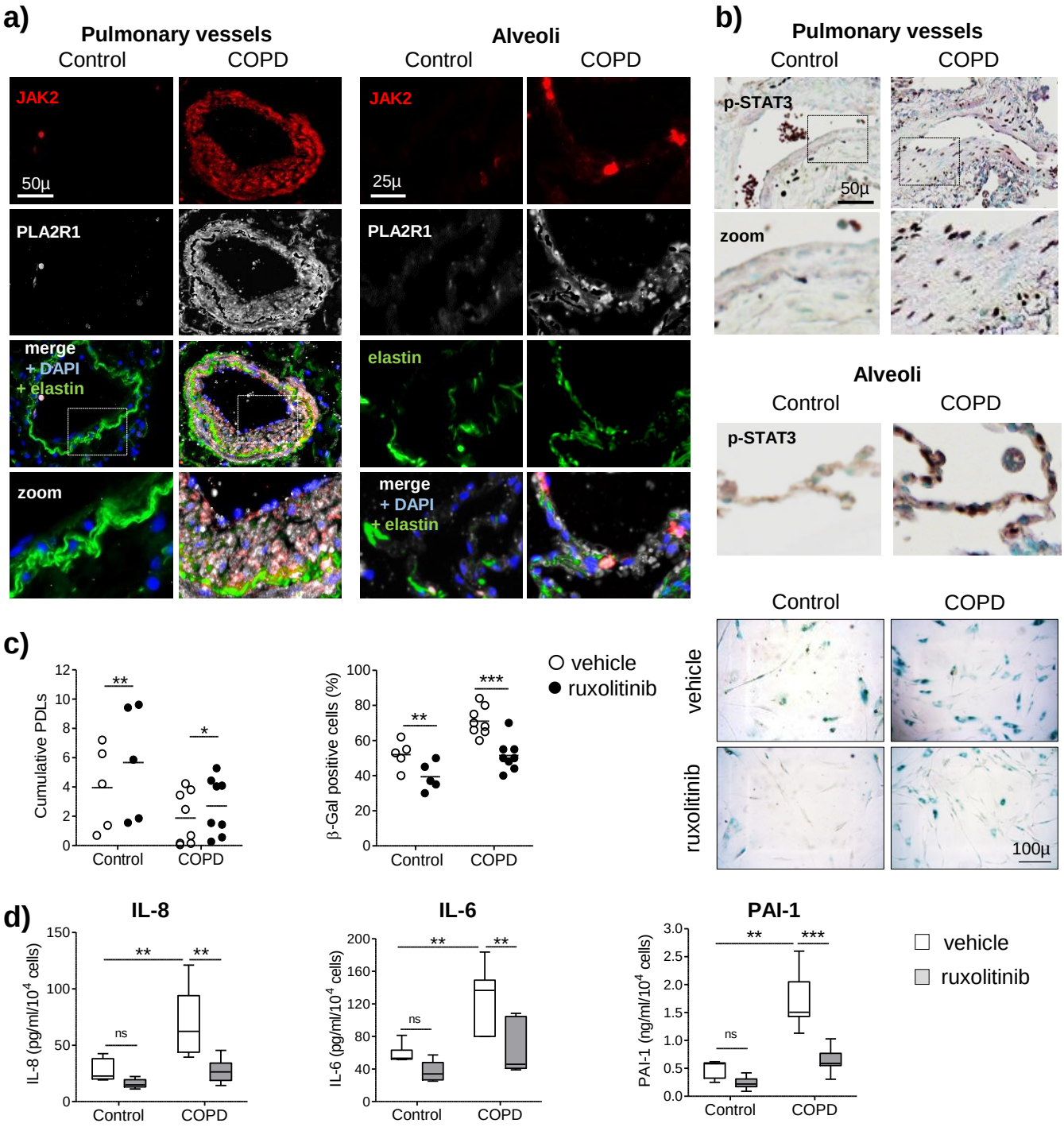

Figure 6: Effects of treatment with ruxolitinib on senescence of cultured PA-SMCs from patients with COPD and controls
(a) Representative micrographs of lung tissue from patients with COPD and controls showing immunofluorescent of JAK2 (red) and PLA2R1 (white) in pulmonary vessels and alveoli. Elastin autofluorescence (green). Nuclei were labeled with DAPI (blue). **(b)** Representative micrographs showing phospho-STAT3 positive cells (brown) in vessels and alveoli. **(c)** Effect of continuous ruxolitinib treatment on senescence of PA-SMCs from patients with COPD (n=8) and controls (n=5) as assessed by the number of PDLs and the percentage of β-Gal-positive cells at passage 6. Typical cells stained for β-Gal are shown on the right. **P*<0.05, ***P*<0.01, ****P*<0.001, two-way ANOVA with Bonferroni's multiple comparisons test. **(d)** Protein levels of IL-8, IL-6, and PAI-1 in conditioned media of cells from patients with COPD and controls treated with ruxolitinib or its vehicle. Data are shown as the median (interquartile range) of 5 values per group. Bars represent extreme values. ***P*<0.01, ****P*<0.001 compared with control, two-tailed Mann Whitney test.

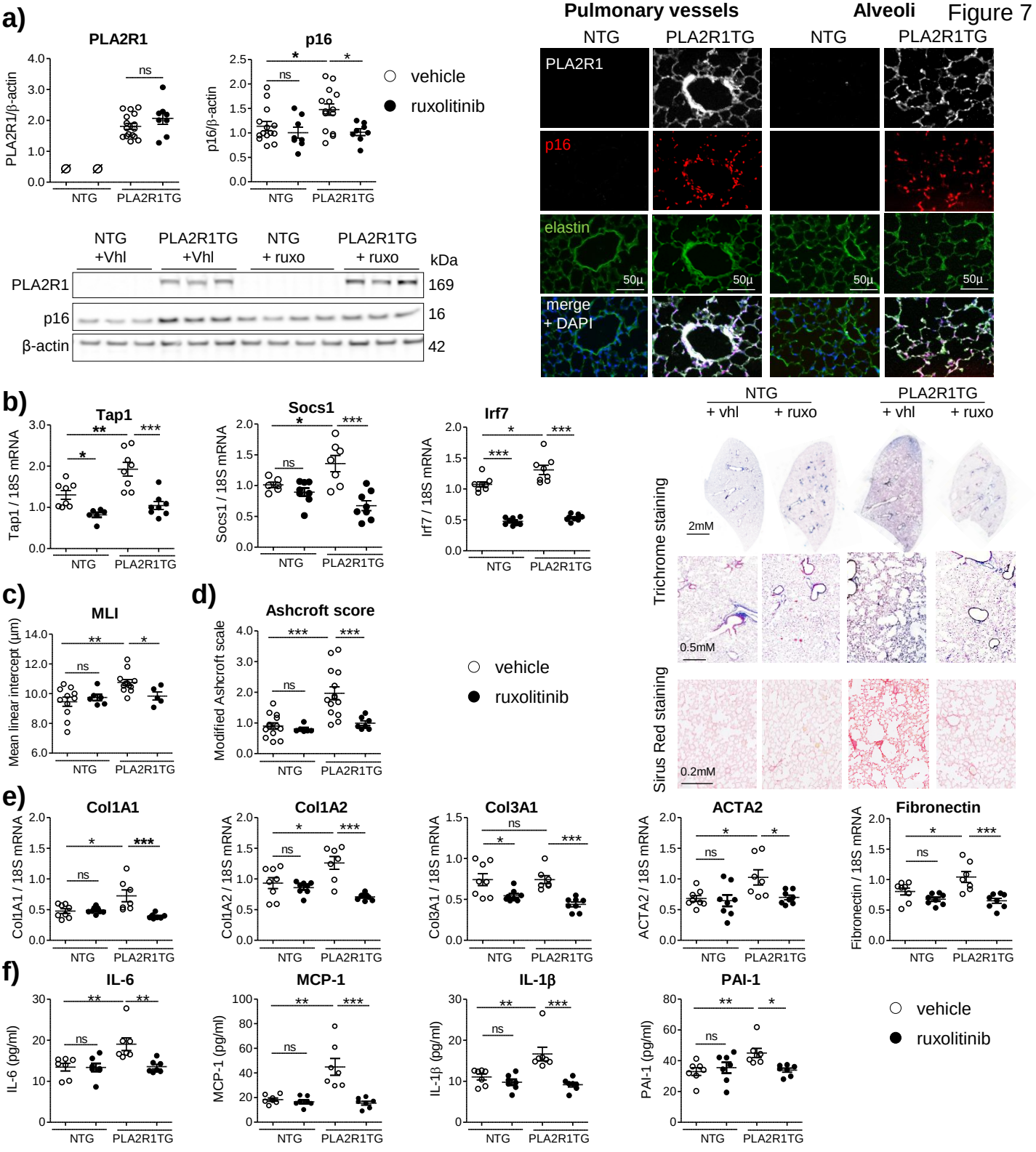

Figure 7: Lung characteristics of transgenic mice constitutively expressing the human *PLA2R1* gene (*PLA2R1*-TG) and their littermates (NTG) subjected to 15 days of ruxolitinib treatment

(a) Lung protein levels of PLA2R1 and p16 in *PLA2R1*-TG (n=16) and NTG (n=15) mice treated with ruxolitinib (75 mg/kg/day) or its vehicle, with their representative immunoblots below. Representative micrographs of lung tissue from *PLA2R1*-TG and NTG showing co-localization of PLA2R1 (white) and p16 (red) in pulmonary vessels and alveoli shown on the right **(b)** Lung mRNA levels of the JAK2 signaling target genes Tap1, Socs1, and Irf7 in each condition. **(c)** Lung emphysema as assessed by measurement of the mean linear intercept (MLI) and **(d)** lung fibrosis as assessed by the modified Ashcroft score. Representative images of lungs from the four groups of mice stained with Masson's trichrome (top and middle panels, in blue) and with Sirius Red (bottom panel, in red). **(e)** Lung mRNA levels of collagens 1A1 and A2 (Col1A1, Col1A2), collagen 3A1 (Col3A1), actin alpha 2 (ACTA2), and fibronectin and **(f)** lung protein levels of IL-6,, MCP-1, IL-1β and PAI-1. **P*<0.05, ***P*<0.01 ****P*<0.001. Two-way ANOVA with Bonferroni's multiple comparisons test.

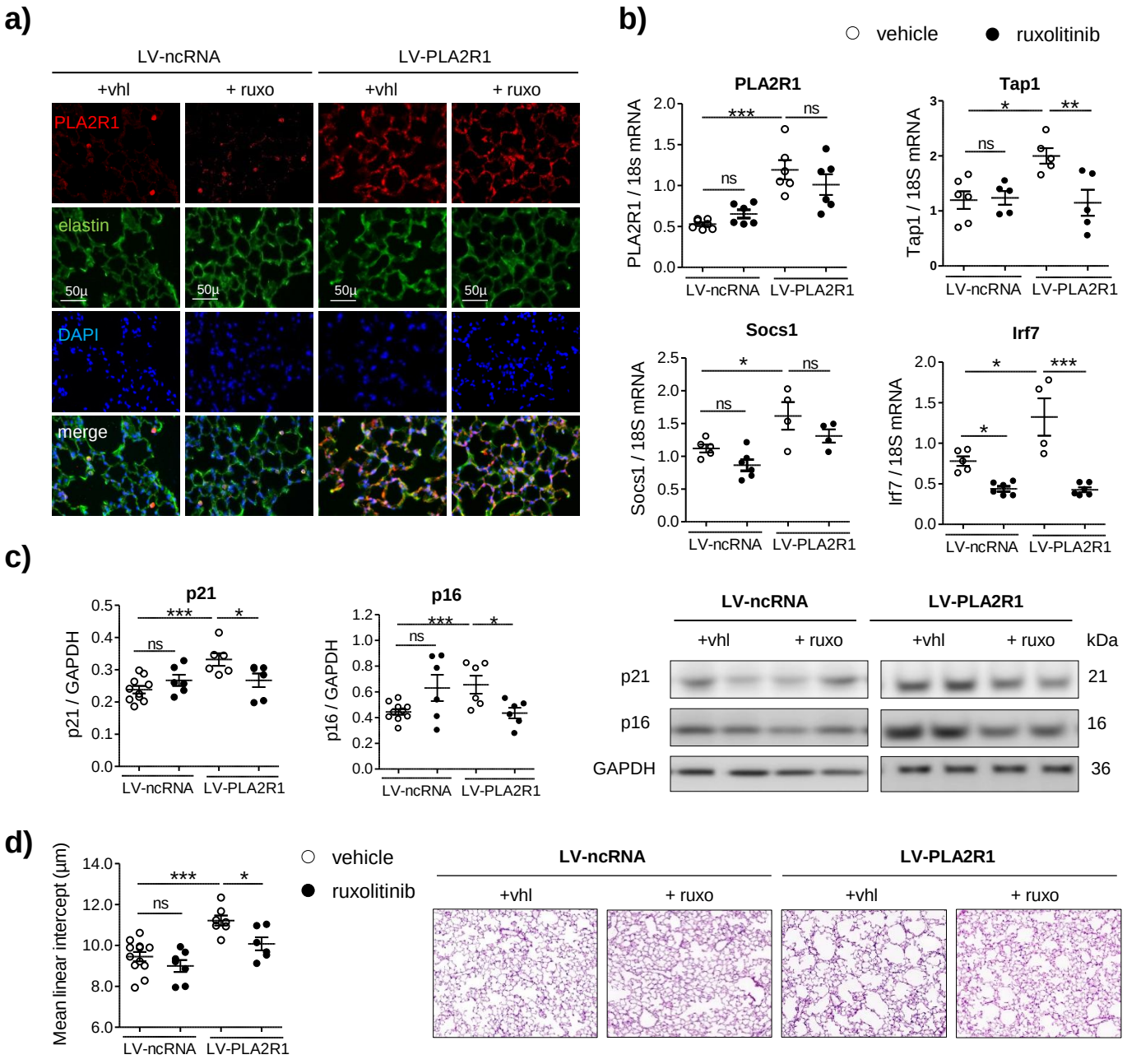

Figure 8: Lung characteristics of mice subjected to intratracheal injection of a lentivirus encoding murine *Pla2r1* gene (LV-*PLA2R1*) **and concomitantly treated with ruxolitinib.**

Mice treated with the LV-*PLA2R1* or a control vector (LV-ncRNA) and simultaneously treated with ruxolitinib (75 mg/kg/day) or vehicle were studied 30 days after the injection. **(a)** Representative micrographs showing *PLA2R1* immunofluorescence (red) in mouse lung sections. **(b)** Lung mRNA levels of *PLA2R1* and of the JAK2 signaling target genes Tap1, Socs1, and Irf7. **(c)** Lung protein levels of p21 and p16 with representative immunoblots in the indicated groups **(d)** Lung emphysema as assessed by measurement of the mean linear intercept (MLI) in hematoxylin and eosin-stained lung sections. **P*<0.05, ***P*<0.01 ****P*<0.001. Student's *t*-test; two-way ANOVA with Bonferroni's multiple comparisons test.

Phospholipase A2-Receptor 1 Promotes Lung-Cell Senescence and Emphysema in Obstructive Lung Disease

D Beaulieu[1], A Attwe[1, 4], M Breau[1], L Lipskaia[1], E Marcos[1], E Born[1], J Huang[1], S Abid[1], G Derumeaux[1], A Houssaini[1], B Maitre[1], M Lefevre[2], N Vienney[1], P Bertolino[3], S Jaber[3], H Noureddine[4], D Goehrig[3], D Vindrieux[3], D Bernard[3], S Adnot[1*]

D Bernard and S Adnot are co-senior authors of this study.

D Beaulieu and A Attwe contributed equally to this study.

METHODS

Study design

The global objectives of the present study were to demonstrate that PLA2R1 is a major player in the process of lung-cell senescence in COPD, to assess JAK/STAT inhibition as a strategy to counteract PLA2R1 effects on cell senescence, and then to validate these findings in preclinical mouse models. To this end, we first assessed PLA2R1 expression in lungs and cells from 23 patients with COPD and 23 controls and investigated whether PLA2R1 colocalized with senescence and DNA-damage markers. We then evaluated the effects of PLA2R1 on replicative cell senescence in several cell types -- pulmonary endothelial cells (P-ECs) and smooth muscle cells (SMCs) -- from 8 patients with COPD and 10 controls. The cells were infected either by retroviral vectors encoding *PLA2R1*, shRNA against *PLA2R1*, or shRNA against *p53*; or by control vectors. Because we previously demonstrated that the prosenescent effects of PLA2R1 involved JAK2, we then tested whether pharmacological JAK1/2 inhibition (by ruxolitinib) induced in vitro inhibition of cell senescence and of the senescence-associated secretory phenotype (SASP), using cells transduced with the retroviral vector encoding *PLA2R1* gene. Finally, we assessed the lung phenotypes of mice expressing the human *PLA2R1* gene (*PLA2R1*-TG mice) under the control of the CMV promoter (40 mice) and of mice injected intratracheally with a mouse *PLA2R1*-encoding lentiviral vector (40 mice), with both mouse models being subjected to *in vivo* ruxolitinib treatment.

Patients and controls

The study was approved by the institutional review board of the Henri Mondor Teaching Hospital, Créteil, France. All patients and controls signed an informed consent document before study inclusion.

Lung tissue samples were obtained from 46 patients who underwent lung resection surgery at the *Institut Mutualiste Montsouris*, Paris, France. Among them, 23 had COPD and 23 were control smokers matched to the COPD patients on age and sex (Table 1). Inclusion criteria for the patients with COPD were an at least 10 pack-year smoking history and a ratio of forced expiratory volume in 1 second (FEV_1) over forced vital capacity (FVC) <70%. The controls had to have a smoking history greater than 5 pack-years; an FEV_1/FVC ratio greater than 70%; and no evidence of chronic cardiovascular, hepatic, or renal disease. None of the patients had a history of cancer chemotherapy. Lung tissue samples collected during surgery were either immediately immersed in DMEM medium then either used for primary cultures of pulmonary artery smooth muscle cells (PA-SMCs) and pulmonary artery endothelial cells (PA-ECs) or immediately snap-frozen in liquid nitrogen then stored at -80°C until protein extraction. In addition, a fragment of lung tissue was fixed in 4% paraformaldehyde aqueous solution (Sigma Aldrich, St Louis, MI) and used for paraffin embedding. Cells were cultured from a subset of 8 patients and 10 controls.

Mice

Adult male mice (C57Bl/6j) were used according to institutional guidelines, which complied with national and international regulations. All animal experiments were approved by the Institutional Animal Care and Use Committee of the French National Institute of Health and Medical Research (INSERM)–Unit 955, Créteil, France. To study the effects of *PLA2R1* overexpression, we generated mice with constitutive expression of the human *PLA2R1* gene placed under the control of the CMV promoter. Their wild-type littermates served as controls (non transgenic mice, NTG). To investigate the effect of lung *PLA2R1* overexpression, mice were injected intratracheally with a lentiviral vector encoding the murine *PLA2R1* gene under the control of the CMV promoter (LV-PLA2R1, Vector ID:

VB180531-1152skr; VectorBuilder Inc., Chicago, IL) or with a control lentiviral non-coding RNA expression vector (LV ncRNA, Vector ID: VB180531-1150skr, VectorBuilder Inc.). Each mouse was injected with 50 µL of lentivirus solution (10^9 TU/ml diluted in DPBS with 5% of Lipofectamine 2000 (Invitrogen, Carlsbad, CA). In preparatory experiments, we identified lung lentivirus-transduced cells by using a lentiviral vector encoding the mCherry reporter gene under the control of the CMV promoter (LV-mCherry). To assess the *in vivo* effect of the JAK1/2 inhibitor ruxolitinib, mice were treated with 75 mg/kg/day of ruxolitinib or vehicle (5% N,N-Dimethylacetamide, 0.5% methyl cellulose from Sigma-Aldrich) given by gavage. Ruxolitinib used for the animal studies was purchased from Clinisciences (Med Chem Express, Monmouth Junction, NJ).

Animal studies, lung tissue analysis

Mice were anesthetized with an intraperitoneal injection of ketamine (60 mg/kg) and xylazine (10 mg/kg). Right ventricular systolic pressure (RVSP) was measured as described previously. The RV was dissected from the left ventricle (LV) plus septum (LV+S), and these dissected samples were weighed to determine the Fulton index (RV/ [LV+S]). The right lung was quickly removed and divided into two parts, which were immediately snap-frozen in liquid nitrogen then stored at -80°C until total RNA and protein extraction for real-time quantitative polymerase chain reaction (RT-qPCR), Western blot, and ELISA. The left lungs were fixed by intratracheal infusion of 4% paraformaldehyde aqueous solution (Sigma Aldrich) at a transpleural pressure of 30 cmH_2O and processed for paraffin embedding. For morphometry studies, 5 µm-thick sagittal sections along the greatest axis of the left lung were cut in a systematic manner and stained with hematoxylin and eosin. Alveolar and vascular morphometry studies were performed by an observer blinded to treatment and genotype, as described elsewhere.

Lung emphysema was assessed on hematoxylin and eosin sections using the mean-linear-intercept (MLI) method described by Knudsen L et al [1]. Light microscope fields were quantified at an overall magnification of 400, using a 42-point and 21-line grid. We examined 20 fields/animal using a systematic sampling method from a random starting point. To correct area values for shrinkage associated with fixation and paraffin processing, we multiplied them by 1.22, as calculated during a previous study.

Lung fibrosis was evidenced on lung sections stained with Masson's trichrome (HT15-1KT, Sigma-Aldrich) and quantified on lung sections stained with Sirius Red (Picro Sirius Red Stain Kit, ab150681, Abcam, Cambridge, UK) using the modified Ashcroft scale [2]. Briefly, the lungs were scanned microscopically with a 20-fold objective, which allowed the evaluation of fine structures while also providing a sufficiently broad view. The entire section was examined by inspecting each field in a raster pattern. Areas with dominating tracheal or bronchial tissue were omitted. The grades were summarized and divided by the number of fields to obtain a fibrotic index for the lung.

For vascular morphometry, each vessel was categorized as non-muscular (no evidence of vessel wall muscularization), partially muscular, or fully muscular. The percentage of muscular pulmonary vessels was determined by dividing the sum of partially and fully muscular vessels by the total number of vessels in the relevant group of animals, as described previously [3].

To measure the release of cytokines IL-6, MCP-1, IL-1β, and PAI-1 from the lung, we used the Quantikine ELISA kit (R&D systems, Minneapolis, MN) according to the manufacturer's instructions.

Cultured cells from patients and controls

P-ECs and PA-SMCs were collected from the lung samples of 8 patients with COPD and 10 controls and cultured as described previously [4, 5]. The cells were then subjected to repeated passages to determine their replicative senescence threshold and population doubling level (PDL). At each passage, cells at 80%-90% confluence were counted in a hemocytometer using trypan blue. The onset of replicative senescence was defined as cessation of cell division, labeling for senescence-associated *beta*-galactosidase, and cell morphology criteria. PDL was computed as follows: PDL = $(\log_{10}Y - \log_{10}X)/\log_{10}2$, where X was the initial number of seeded cells and Y the final number of cells [5, 6].

To assess the effect of JAK/STAT inhibition by ruxolitinib, cells from patients with COPD and controls were continuously cultured in medium containing either vehicle or ruxolitinib (0.5 μM). The effects of ruxolitinib on cell senescence were evaluated comparatively with those of the vehicle.

We specifically designed experiments to assess the effects of *PLA2R1* inhibition on replicative cell senescence. Cells from patients with COPD and controls were infected with either a retroviral vector encoding short hairpin RNAs targeting *PLA2R1* (shPLA2R1) or a control vector (shControl), as previously described [7]. We then compared the effects of *PLA2R1* knockdown to those of the control vector [8]. The infection protocols were designed to infect nearly all the cells, as demonstrated by fluorescence observed with a GFP-expressing retroviral vector (not shown).

In further specific experiments, cells from patients were infected with a retroviral vector encoding human *PLA2R1* (PLA2R1 virus) or with a control vector as previously described [7, 8]. We then compared the effects of *PLA2R1 overexpression* to those of the control vector. In these experiments, cells were continuously cultured in a medium containing either vehicle or the JAK1/2 inhibitor ruxolitinib (0.5 μM).

For analysis of cultured cells at early and late passages, cells were placed in reduced media containing 0.2% FBS for 24 h for P-ECs or 48 h for PA-SMCs, as previously described [4, 5]. Then, the cells were collected for further RNA and proteins analysis and to determine the percentage of *beta*−galactose-positive cells. The conditioned media were collected and used to quantify IL-8, IL-6, and PAI-1 using Quantikine ELISA kits (R&D systems, Minneapolis, MN) according to the manufacturer's instructions.

Senescence-associated beta-galactosidase staining

At each passage, cells at 60% confluence were fixed with 2% formaldehyde and 0.2% glutaraldehyde for 10 minutes. Then, the cells were washed with PBS and stained in a titrated pH6 solution containing 40 mM citric acid, 150 mM NaCl, 2 mM $MgCl_2$, 5 mM potassium ferrocyanide, and 1 mg/mL X-Gal.

Immunofluorescence

For immunofluorescence, cells were fixed for 10 minutes in methanol. Paraffin-embedded sections of lung were deparaffinized using xylene and a graded series of ethanol dilutions then processed for epitope retrieval using citrate buffer (0.01 M, pH 6; 90°C, 20 min). For PLA2R1 epitope retrieval, we used NeoUltra retrieval solution (NB-23-00178-4, NeoBiotech, Nanterre, France) according to the manufacturer's instructions. For nuclear immunolabeling, tissues were permeabilized with 0.1% Triton X-100 in PBS for 10 minutes.

Saturation was achieved using Dako antibody diluents with 10% goat serum. For double staining, first and second primary antibodies were diluted in Dako antibody diluents with 3% goat serum then incubated for 1 hour at 37°C in a humidified chamber. After PBS washes, the sections were covered with secondary antibody (mixed with mouse, rabbit, rat, or chicken Alexa Fluor® 480, Alexa Fluor® 555, or Alexa Fluor® 660 [Abcam]) for 40 minutes at 37°C in

a humidified chamber. After 5 minutes of staining with DAPI, the sections were protected with coverslips secured with fluorescent mounting medium.

Fluorescence was recorded using an Axio Imager M2 imaging microscope (Zeiss, Oberkochen, Germany) and analysed on digital photographs using Image J software (imagej.nih.gov/ij/).

Immunohistochemistry

For immunohistochemistry on paraffin-embedded sections, after deparaffinization and antigen retrieval, the endogenous peroxidase activity was blocked with 3% H_2O_2 and 10% methanol in PBS for 10 minutes. Permeabilization was done using 0.1% Triton X-100 in PBS for 10 minutes. Saturation was achieved by incubation for 30 minutes at 37°C in antibody diluent (ref.NB-23-00171-1, NeoBiotech) supplemented with 12% of goat serum. The slides were then incubated for 60 minutes at 37°C with primary antibody. The secondary antibody consisted of Sav-HRP conjugates. DAB substrate solution was used to reveal the color of the antibody staining. Nuclear counterstaining was achieved with methyl green.

Protein extraction and immunoblotting

Total proteins were extracted using RIPA lysis buffer (10 mM sodium phosphate pH 8, 150 mM NaCl, 1% sodium deoxycholate, 1% NP40, 0.5% SDS, 1 mM PMSF, 10 mM NaF, 1 mM sodium orthovanadate, and protease inhibitor cocktail [Roche, Meylan, France]). Immunoblots were carried out using the indicated antibodies and detected using an enhanced chemiluminescence detection system (GE Healthcare, Little Chalfont, UK). Densitometric quantification was normalized for the *beta*-actin or GAPDH level using GeneTools software (Ozyme, Montigny le Bretonneux, France).

Real-time quantitative PCR (RT-qPCR)

Total RNA from tissues and cells was extracted with the RNeasy Plus Mini Kit (Qiagen, Courtaboeuf, France) according to the manufacturer's instructions. The RNA concentration was assessed using a Nanodrop ND-1000 spectrophotometer (Thermo Fisher Scientific, Les Ulis, France), and RNA integrity was confirmed by electrophoresis. One µg of total RNA was used for cDNA synthesis using SuperScript II Reverse Transcriptase (Thermo Fisher Scientific). The quantitative PCR was performed in triplicate with TaqMan Probes (TaqMan Gene Expression assays, Applied Biosystems, Illkirch, France) and TaqMan Fast Advanced Master Mix (Thermo Fisher Scientific) in the QS6, QuantStudio 6 Flex Real-Time PCR system (Applied Biosystems, Illkirch, France). All data were analysed using QuantStudio Real-Time PCR software (Applied Biosystems). The relative expression level of target genes was calculated by the ΔΔCt method and normalized to the reference genes 18s and SF3A1.
The TaqMan Gene Expression assays used for human and mouse cells are described in supplemental Table S3.

Materials

The JAK1/2 inhibitor ruxolitinib used for animal studies was purchased from Clinisciences (Med Chem Express).

The following primary antibodies were used: mouse monoclonal anti-PLA2R1 antibody (1:200, ab211490, Abcam); rabbit polyclonal anti-PLA2R1 antibody (1:200, ab194256, Abcam); rabbit polyclonal anti-PLA2R1 antibody (1:200, abx129773, ABBEXA); mouse monoclonal anti-CDK2A/p16INK4a (p16, ab54210, Abcam), polyclonal rabbit anti-α-smooth muscle actin (αSMA) antibody (1:400, ab5694, Abcam), polyclonal rabbit anti-CD31 (PECAM) antibody (1:20, ab28364, Abcam), monoclonal rabbit anti-MUC1 (1:200, ab109185, Abcam antibody); polyclonal rabbit anti-53BP1 antibody (1:200, NB100-304,

Novus Biologicals, Littleton, CO); phospho-gamma-H2AX (Ser139) recombinant rabbit monoclonal antibody (RM224) (# MA5-33062, RRID AB_2810155, Thermo Fisher Scientific); polyclonal mouse anti-proliferating cell nuclear antigen antibody, anti-PCNA (1:200, ab29, Abcam); monoclonal mouse anti-JAK1 antibody (1:200; sc-1677, Santa Cruz Biotechnology), polyclonal rabbit anti-JAK2 antibody (1:200, sc-294, Santa Cruz Biotechnology), goat polyclonal anti-phospho STAT3 (Tyr705) antibody 1:200, sc-7993, Santa Cruz Biotechnology); rabbit polyclonal anti-phospho-Jak2 (Tyr1007/1008) antibody (1:200, y #3771, Cell Signaling), rabbit anti-vimentin antibody (1:500, ab92547, Abcam), rabbit anti-fibroblast-specific protein antibody (1:200, ab27957, Abcam), anti-beta-Actin (β-Act, A5316, Sigma); GAPDH (sc-25778); anti-CDK2A/p16INK4a (p16, 92803, Cell Signaling; p16, PA520379, Thermo Scientific); anti-p21 Waf1/Cip1 (p21, 2946, Cell Signaling Technology)

Statistical analysis

Quantitative variables are expressed as individual values and mean or as median (range). Statistical analyses were performed with GraphPad Prism 7 software following the guidelines in GraphPad Prism. One-way analysis of variance (ANOVA) or two-way ANOVA followed by Bonferroni's multiple comparisons test were used to compare the means of more than two independent groups. Values represented as medians (interquartile range) were compared by the nonparametric Kruskal-Wallis test. *P* values less than 0.05 were considered significant.

References

1. Knudsen L, Weibel ER, Gundersen HJ, Weinstein FV, Ochs M. Assessment of air space size characteristics by intercept (chord) measurement: an accurate and efficient stereological approach. *J Appl Physiol (1985)* 2010: 108(2): 412-421.

2. Hubner RH, Gitter W, El Mokhtari NE, Mathiak M, Both M, Bolte H, Freitag-Wolf S, Bewig B. Standardized quantification of pulmonary fibrosis in histological samples. *Biotechniques* 2008: 44(4): 507-511, 514-507.

3. Mouraret N, Houssaini A, Abid S, Quarck R, Marcos E, Parpaleix A, Gary-Bobo G, Dubois-Rande JL, Derumeaux G, Boczkowski J, Delcroix M, Blasco MA, Lipskaia L, Amsellem V, Adnot S. Role for telomerase in pulmonary hypertension. *Circulation* 2015: 131(8): 742-755.

4. Noureddine H, Gary-Bobo G, Alifano M, Marcos E, Saker M, Vienney N, Amsellem V, Maitre B, Chaouat A, Chouaid C, Dubois-Rande JL, Damotte D, Adnot S. Pulmonary artery smooth muscle cell senescence is a pathogenic mechanism for pulmonary hypertension in chronic lung disease. *Circ Res* 2011: 109(5): 543-553.

5. Amsellem V, Gary-Bobo G, Marcos E, Maitre B, Chaar V, Validire P, Stern JB, Noureddine H, Sapin E, Rideau D, Hue S, Le Corvoisier P, Le Gouvello S, Dubois-Rande JL, Boczkowski J, Adnot S. Telomere dysfunction causes sustained inflammation in chronic obstructive pulmonary disease. *Am J Respir Crit Care Med* 2011: 184(12): 1358-1366.

6. Nogueira V, Park Y, Chen CC, Xu PZ, Chen ML, Tonic I, Unterman T, Hay N. Akt determines replicative senescence and oxidative or oncogenic premature senescence and sensitizes cells to oxidative apoptosis. *Cancer Cell* 2008: 14(6): 458-470.

7. Augert A, Payre C, de Launoit Y, Gil J, Lambeau G, Bernard D. The M-type receptor PLA2R regulates senescence through the p53 pathway. *EMBO Rep* 2009: 10(3): 271-277.

8. Vindrieux D, Augert A, Girard CA, Gitenay D, Lallet-Daher H, Wiel C, Le Calve B, Gras B, Ferrand M, Verbeke S, de Launoit Y, Leroy X, Puisieux A, Aubert S, Perrais M, Gelb M, Simonnet H, Lambeau G, Bernard D. PLA2R1 mediates tumor suppression by activating JAK2. *Cancer Res* 2013: 73(20): 6334-6345.

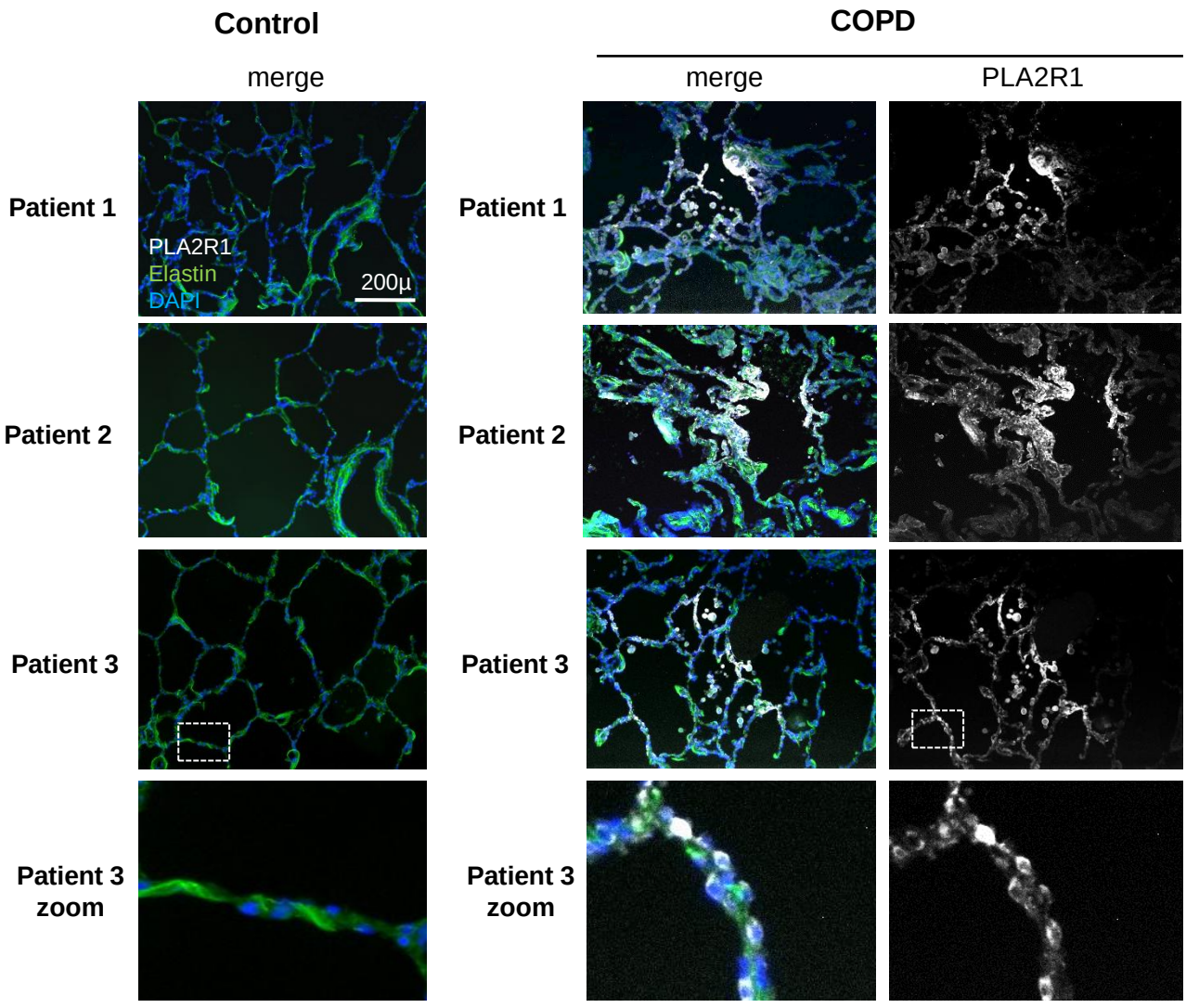

Supplemental Figure 1
Distribution of PLA2R1 immunofluorescence activity in lungs from patients with COPD and controls
Representative micrographs of lung tissue from 3 patients with COPD and 3 controls showing PLA2R1 expression (white), and merge with elastin autofluorescence (green) and nuclear DAPI staining (blue). The zoom area is indicated by a square.

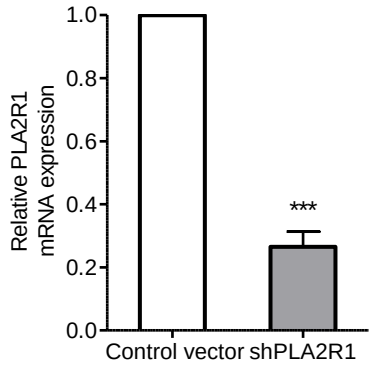

S**upplemental Figure 2:** *PLA2R1* mRNA levels measured in cells stably infected with the sh*PLA2R1*-encoding retroviral vector, compared to cells infected with the control vector. ****P*<0.001 for comparison between groups, Student's *t*-test

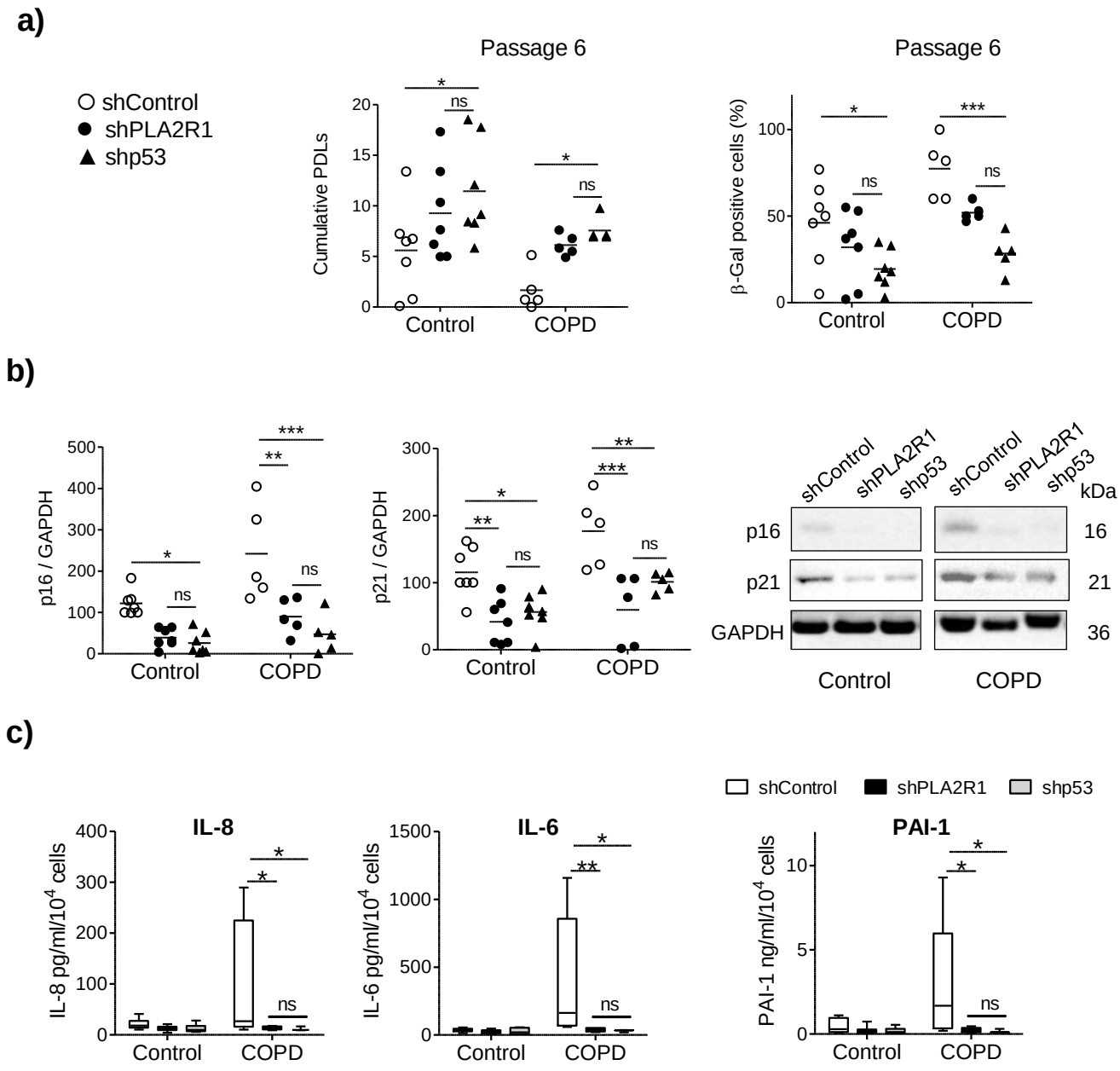

Supplemental Figure 3

Comparison between inactivation of *PLA2R1* and *p53* in cells from patients with COPD and controls

Cells from patients with COPD (n=5) and controls (n=5) were infected either with a retroviral vector encoding an shRNA that targeted *PLA2R1* (sh*PLA2R1*) or *p53* (sh*p53*) or with a control vector encoding a scramble sequence (shControl). The cells were then subjected to successive passages. **(a, b)** Graphs showing cumulative numbers of PDLs, percentage of β-Gal-positive cells, and p16 and p21 protein levels as assessed by Western blotting, all determined at passage 6 are shown as individual values with the mean. Representative immunoblots are shown on the right. **P*<0.05, ***P*<0.01, ****P*<0.001 vs. shControl, two-way ANOVA with Bonferroni's multiple comparisons test. **(c)** Protein levels of IL-8, IL-6, and PAI-1 in PA-SMC-conditioned media at passage 6. Data are shown as median (interquartile range) of 5 values per group. Bars represent extreme values. There were no significant differences between values recorded in cells treated with the sh*PLA2R1* or the sh*p53* vectors. **P*<0.05, ***P*<0.01 vs. shControl one-tailed Mann Whitney test.

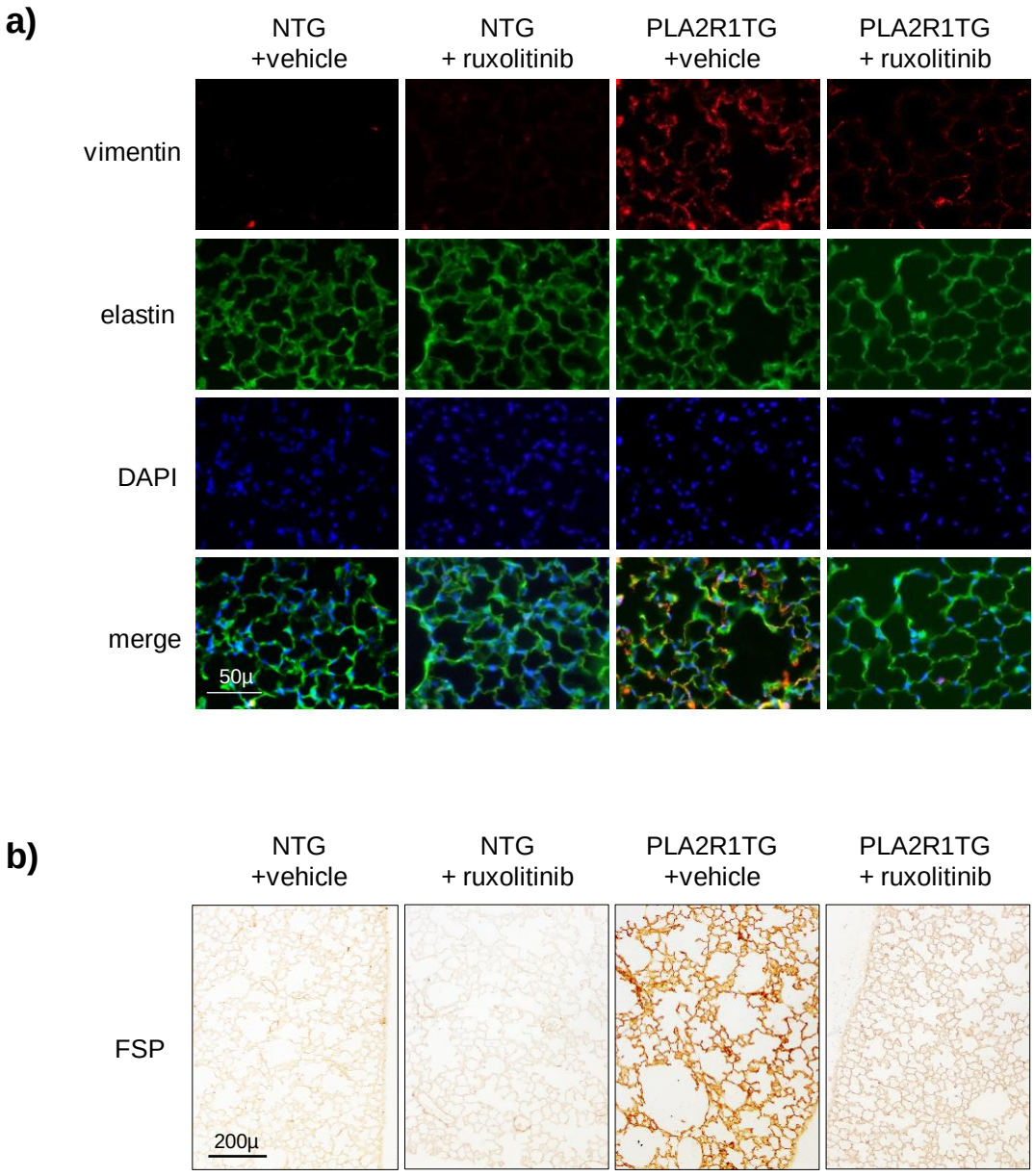

Supplemental Figure 4
Lung vimentin and fibroblast-specific protein (FSP) immunostaining in *PLA2R1*TG mice and littermate controls subjected to 15 days of treatment with ruxolitinib or vehicle.
(a) Representative micrographs showing lung sections stained for vimentin (red), a lung alveolar fibroblast marker, in *PLA2R1*-TG and control mice treated with ruxolitinib or vehicle. Elastin autofluorescence (green); the nuclei were stained with DAPI (blue). **(b)** Representative micrographs showing lung sections stained for fibroblast-specific protein (FSP, brown), a lung alveolar fibroblast marker, in the same groups of mice.

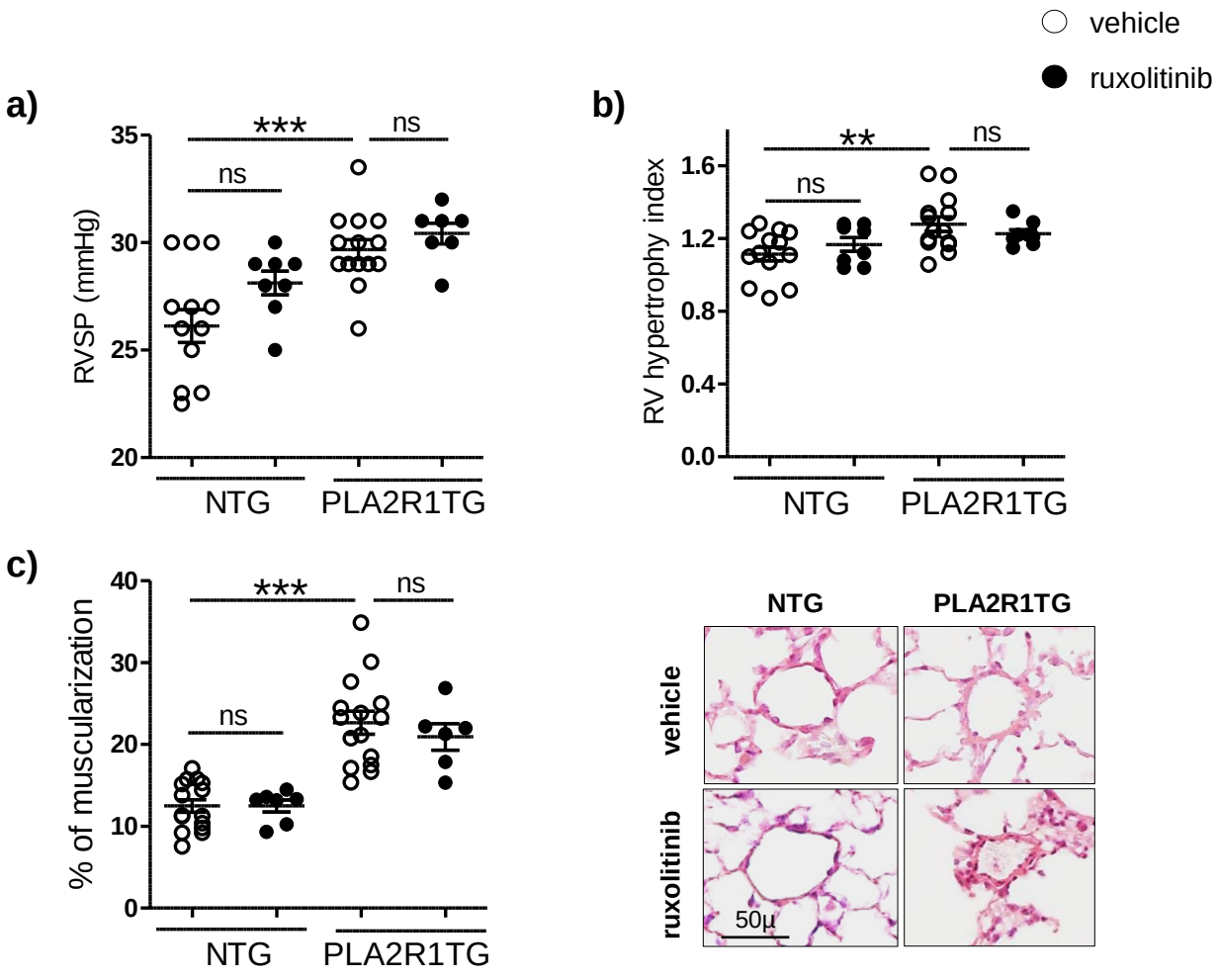

Supplemental Figure 5. **Pulmonary hemodynamic parameters in *PLA2R1*TG and littermate control (NTG) mice subjected to 15 days of treatment with ruxolitinib or vehicle**

(a) Right ventricular systolic pressure (RVSP) **(b)** Right ventricular hypertrophy index (Fulton's index) **(c)** Muscularization of pulmonary vessels (percent of muscularized vessels over the total number of pulmonary vessels) and representative images of pulmonary vessels. Graphs represent individual values with the mean±SEM. ***P*<0.01, ****P*<0.001 for comparisons between groups as indicated. Unpaired Student's *t*-test and two-way ANOVA with Bonferroni's multiple comparisons test.

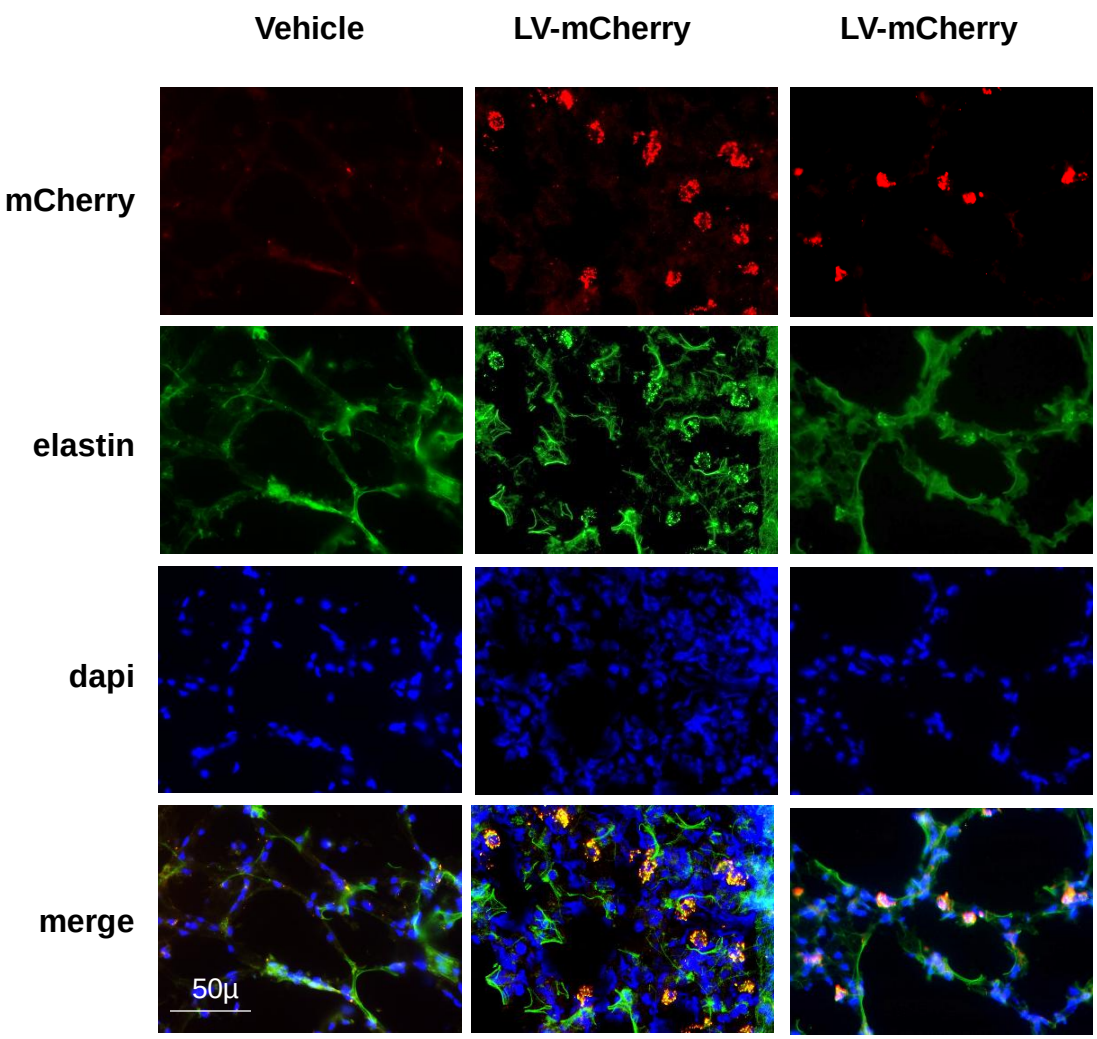

Supplemental figure 6. Identification of lentivirus-transduced cells in the mouse lung.
A lentiviral vector encoding the mCherry gene under the control of the CMV promoter (LV-mCherry) was injected intratracheally to mice (109 TU/ml diluted in DPBS with 5% of Lipofectamine 2000) in comparison with vehicle (DPBS with 5% of Lipofectamine 2000). , Mice were sacrificed on day 9 post-infection, and lung cryosections were assessed by fluorescence microscopy for mCherry reporter gene expression (red). Green – elastin autofluorescence, nuclei were stained with DAPI (blue). Bar – 50µm.

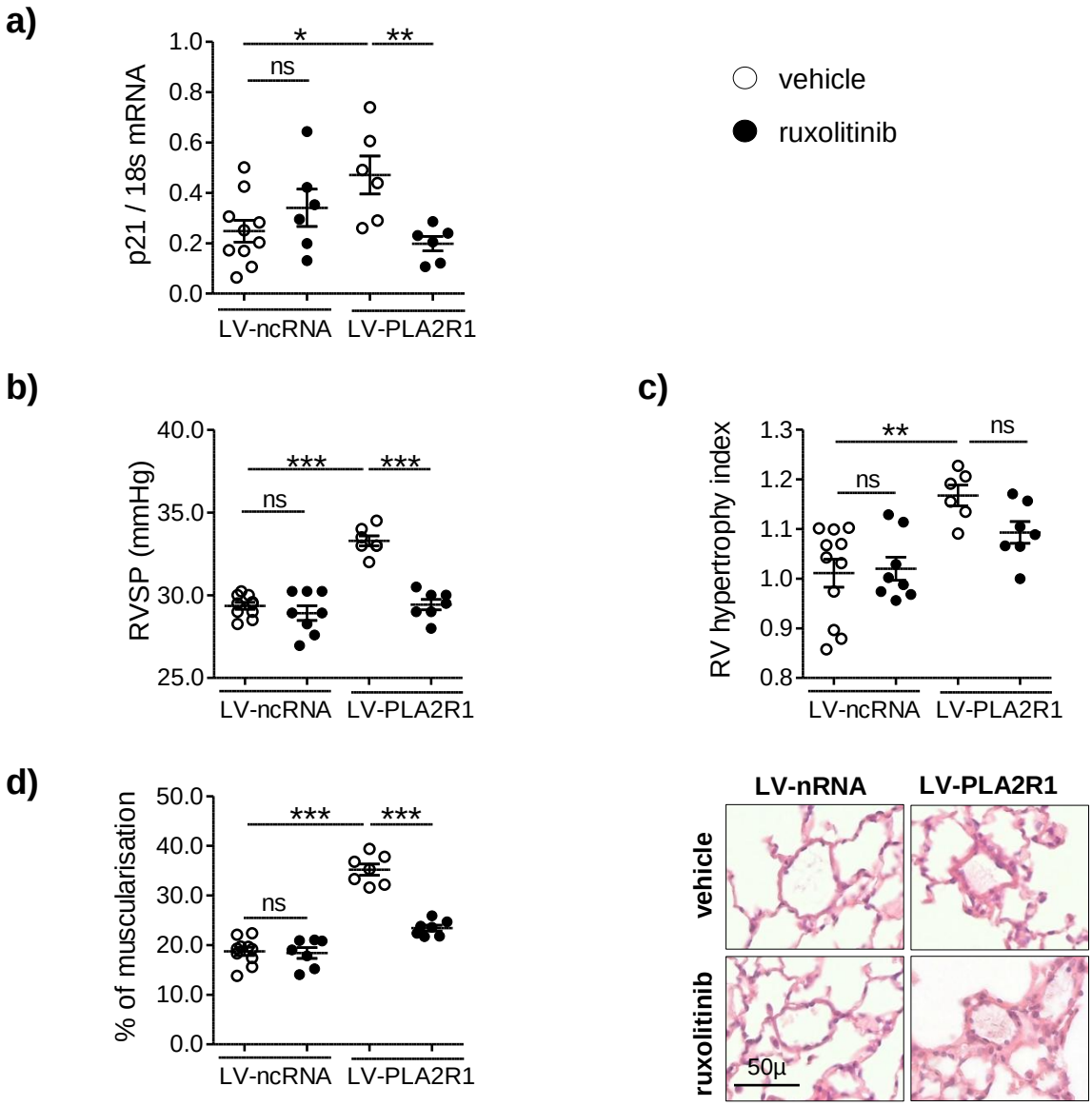

Supplemental Figure 6

Pulmonary hemodynamic parameters in mice subjected to an intratracheal injection of a lentivirus encoding the mouse *Pla2r1* gene (LV-*PLA2R1*) and concomitantly treated with ruxolitinib

Mice treated with the LV-*PLA2R1* or a control vector (LV-ncRNA) and simultaneously treated with ruxolitinib (75 mg/kg/day) or vehicle were studied 30 days after the injection. **(a)** Lung mRNA level of p21 **(b)** Right ventricular systolic pressure (RVSP) **(c)** Right ventricular hypertrophy index (Fulton's index) **(d)** Muscularization of pulmonary vessels (percent of muscularized vessels over the total number of pulmonary vessels) and representative images of pulmonary vessels. Graphs represent individual values with the mean±SEM. ***P*<0.01, ****P*<0.001 for comparisons between groups as indicated. Student's *t*-test and two-way ANOVA with Bonferroni's multiple comparisons test.

Table S1

	Control		COPD	
	Mean	*sem*	Mean	*sem*
n	23		23	
Age, yr	65,17	±*2,60*	59,83	±1,27
FEV %	92,39	±*2,20*	77,78	±3,43
FVC%	96,23	±*2,98*	88,73	±5,10
FEV /FVC, %	82,74	±*1,89*	66,05	±1,13
Pack-years	25,74	±*4,76*	44,76	±5,23

Table S2

	Control		COPD	
	Mean	*sem*	Mean	*sem*
n	10		8	
Age, yr	62,72	±*4,27*	64,7	±*2,32*
FEV %	94,38	±*2,73*	69,78*	±*3,23*
FVC%	101,17	±*1,69*	80,67	±*5,97*
FEV/FVC,%	83,85	±*3,30*	62,2**	±*2,25*
Pack-years	19	±*5,39*	52,78*	±*6,67*

Supplemental Tables S1 and S2

Clinical features and pathological variables of patients with COPD and control smokers. Table S1 describes all patients and controls from whom lung samples were obtained. Cells were collected from a subset of 8 patients and 10 controls, whose characteristics are described in Table S2.

Abbreviations: FEV_1, forced expiratory volume in 1 second; FEV_1%, percentage of the predicted FEV_1 value; FVC, forced vital capacity; FVC%, percentage of the predicted FVC value.

Table S3 : TaqMan Gene Expression assays

Target Gene	Assay ID
hPLA2R1	Hs01073364_m1
mPLA2R1	Mm0476896_m1
p21	Mm04205640_g1
Tap1	Mm00443188_m1
SOCS1	Mm00782550_s1
Irf7	Mm00516793_g1
Col1a1	Mm00801666_g1
Col1a2	Mm00483888_m1
Col3a1	Mm00802300_m1
Acta2	Mm00725412_s1
Fibronectin	Mm01256744_m1

Reference Gene	Assay ID
hSF3A1	Hs01066327_m1
m18s	Mm03928990_g1